

Human-perceived temperature changes linked to local climate zones under extreme hot and cold weathers: A study in the North China Plain

Xiang Li ^a , Ming Luo ^{a,*}, Jianfeng Li ^b, Sijia Wu ^a, Hui Zhang ^a, Ziwei Huang ^a, Qiuting Wang ^a, Wenyue Cao ^a, Yu Tang ^a , Xiaoyu Wang ^a

^a School of Geography and Planning, Sun Yat-sen University, Guangzhou 510006, China

^b Department of Geography and Management, The Chinese University of Hong Kong, Sha Tin, Hong Kong SAR, China



ARTICLE INFO

Keywords:

Local climate zones
Human-perceived temperature
Extreme temperature
Extreme weather
Heat stress
North China Plain

ABSTRACT

Human-perceived temperature (HPT) describes the combined effects of multiple meteorological factors on human body. However, the relationship between HPT, local climate zones (LCZs), and extreme weather events remains unclear, especially for rapidly urbanizing regions including the North China Plain (NCP), one of the most populated regions vulnerable to heat stress. Here, we examine the HPT changes associated with LCZ and temperature extremes by taking NCP as an example. We show that HPT in built-up areas of NCP is warmer than that in natural surfaces, with an average summer heat index of 27.69 °C and 27.26 °C, respectively. Mid- and high-rise buildings exhibit higher HPTs than low-rise. This difference is even larger in denser building agglomerations (0.80 °C in compact areas versus 0.75 °C in open zones). Urban thermal environment is more comfortable in greenery, particularly tree-covered areas. A comparison between normal and extreme weather conditions reveals a remarkable cooling effect by urban greenery. Nevertheless, during extreme heat, urban trees may have diminished cooling and potentially exacerbate humid heat threat, likely via increased water vapor by evapotranspiration. Under extreme conditions, LCZs 7 and 10 demonstrate high HPT variability and vulnerability. These findings provide valuable insights for improving urban climate resilience, landscape planning, and sustainable development.

1. Introduction

Human-induced global warming is 1.1 °C above pre-industrial period (IPCC, 2023). It has exacerbated extreme weather and seriously threatens natural systems and human well-being (Li et al., 2019; Zhang et al., 2023a). Extreme temperature events with increasing intensity and duration pose serious consequences on human health (Luo et al., 2024; Murali et al., 2023; World Health Organization, 2018), with nearly one-third of the global population being exposed to extreme temperatures for at least 20 days per year (Mora et al., 2017). The risk of extreme temperature hazards to humans will further be exacerbated in the future, particularly in densely populated cities (Overland, 2021; Stone et al., 2021). Studies on the thermal environment have extensively focused on air and surface temperatures, and some of them have noticed human-perceived temperature (HPT) (Luo & Lau, 2021b; Vargas Zepetello et al., 2022; Wang et al., 2024).

HPT, known as “feels-like” temperature, can be categorized into

meteorology- and energy-balanced indices (Yilmaz et al., 2023). The former includes heat index (HI) and wind chill temperature (WCT) (Osczevski & Bluestein, 2005; Rothfusz & Headquarters, 1990), and the latter contains mean radiant temperature (T_{mr}), physiologically equivalent temperature (PET), and universal thermal climate index (UTCI) (Bröde et al., 2012; Höppe, 1999; Thorsson et al., 2007). HPT integrates factors such as air temperature, humidity, and wind speed. For examples, high air temperature accompanied by heavier moisture can elevate HPT through hygrothermal stress (Wang et al., 2021). Windy conditions can mitigate urban heat islands and improve outdoor thermal comfort, while on cold days, wind makes temperatures feel cooler than on calm conditions due to the wind chill effect (He et al., 2020; Lin et al., 2019). Meteorology-based HPT indices have gained increasing attention from scholars and have been widely applied in thermal environment assessment studies (Heidari et al., 2024; Luo & Lau, 2021b; Wang & Yi, 2021; Zhang et al., 2023c). It has been demonstrated that HPT is rising faster than air temperature globally, with urbanized and densely populated

* Corresponding author at: School of Geography and Planning, Sun Yat-sen University, No. 132 East Waihuan Road, Panyu District, Guangzhou 510006, China.
E-mail address: luom38@mail.sysu.edu.cn (M. Luo).

areas experiencing more pronounced warming and greater heat stress intensification (Li et al., 2018; Luo & Lau, 2019). However, most previous studies examined HPT based on sparsely distributed meteorological station data or model simulations, typically focusing on a limited set of indices, such as HI, with insufficient consideration of multiple HPT indices (Luo & Lau, 2021a; Yilmaz et al., 2023). By contrast, the development of high-resolution HPT products, such as HiTIC-NCP with daily temporal resolution and 1 km spatial resolution, has significantly advanced research into fine-scale human thermal environment research (Li et al., 2023; Yang et al., 2023; Zhang et al., 2023b). However, the local-scale HPT variations at finer temporal scales (e.g., daily and during extreme weather events) remain limited.

Meteorological factors in the local region are shaped by both climate change and significant land cover alterations (IPCC, 2023; Jendritzky et al., 2012; Lambin et al., 2003; Palanisamy et al., 2024). As cities continue to expand and develop, extensive impervious materials and structures alter the properties of the land surface, contributing to regional climate change (Zhou et al., 2014). The “urban-rural” dichotomy in land cover, commonly used in thermal environment studies, limits the ability to capture the complexity of local land cover and spatial forms, resulting in an incomplete representation of the local climate environment (Zhou et al., 2024). The local climate zones (LCZs) scheme characterizing the regional surface and spatial structure has been proposed to describe detailed urban landscapes (Stewart & Oke, 2012). This scheme comprehensively considers multiple urban local climate influencing factors, including surface coverage (e.g., the proportion of impervious surfaces and vegetation), urban structural characteristics (e.g., sky view factors), surface material differences (e.g., surface reflection rate), and local human activities, and explicitly categorizes the surface into 17 categories (including ten built-up environments and seven natural landscapes) (Stewart & Oke, 2012). By capturing the heterogeneity within cities, LCZs offer a multi-dimensional description of complex urban spaces and facilitate refined research on urban climate, providing a standardized measure for studying local thermal environments (Jiang et al., 2020; Palanisamy et al., 2024; Zhao et al., 2020). Extensive studies (see Table 1) have been conducted to explore human thermal comfort and its mechanisms across limited LCZs in different regions, including Hong Kong and Belgium. However, the limited range of LCZ types results in insufficient exploration of HPT characteristics across different LCZs (Rahmani & Sharifi, 2025). A more comprehensive understanding of the impacts of urban morphology and landscape on HPT is crucial for optimizing urban

planning and improving sustainable city development.

Compared with normal conditions, extreme weather (e.g., heat waves and cold surges) bring about greater variability and complexity in meteorological variables and their interactions, influencing the impact of LCZs on HPT under such conditions (Chen et al., 2023; García, 2022; Li et al., 2018). The LCZ framework effectively reflects local meteorological characteristics in diverse environments, providing insights to identify areas highly exposed and vulnerable to extreme weather at a fine scale (Jiang et al., 2024; Xie et al., 2024). For example, by investigating HPT changes during the transition from normal to extreme hot conditions in Ghent, Belgium, Top et al. (2020) found that compact mid- and low-rise buildings (i.e., LCZs 2 and 3) with the highest daytime and nighttime heat stress respectively on extreme heat days, while dense tree (i.e., LCZ B), usually an urban park, is with the least extreme heat stress. Similarly, Jiang et al. (2024) discovered that when extreme heat comes, high-rise buildings (i.e., LCZs 1 and 4) absorb more solar radiation than other buildings, thus elevating HPT, and sparse low-rise buildings (i.e., LCZ 9) also exhibit pronounced HPT increases during extreme weather. Green spaces provide a cooling effect, increase regional humidity, and enhance near-surface wind speed, offering an effective strategy for mitigating heat stress risks (Yilmaz et al., 2007). However, prolonged high temperatures during extreme heat events elevate air vapor pressure, reducing plant stomatal conductance and transpiration rate (Wang et al., 2019a, 2020), while tree transpiration is affected by changes in saturated vapor pressure under extreme cold conditions (Wang et al., 2019a, 2019b). The specific impacts of extreme temperatures on different LCZs remain uncertain. Moreover, the limited existing studies largely focus on HPT changes during extreme heat, with variations under extreme cold conditions yet to be explored.

As one of the most densely populated and urbanized regions in the world, the North China Plain (NCP) is among the most climate-sensitive areas globally (Kang & Eltahir, 2018; Wang et al., 2021; You et al., 2022). Since 1961, the region has experienced a temperature increase of 0.33 °C per decade, with approximately 660,000 people exposed to summer extreme heat day over the past five decades (China Meteorological Administration, 2023; Samset et al., 2023). The risk of extreme heat events in this region will likely continue to rise in the future (Wang et al., 2022; Wu et al., 2019b). Understanding local-scale heat environments in densely populated and climate-sensitive areas like NCP is essential for mitigating heat-related health risks to residents.

To bridge the aforementioned research gap, this study utilizes HPT indicators from a human thermal index collection (namely, HiTIC-NCP)

Table 1
Review of existing studies on HPTs across different regions.

Authors (Published Year)	Study Area	Dataset	Method	Highlight
Manob & Arijit (2020)	Sriniketan-Santiniketan Panning Area (Bengal)	Questionnaire surveys and field measurements	Coefficient of variation, ANOVA, and correlation	Morphology of outdoor spaces drives local HPT variations.
Karimimoshaver & Shahrok (2022)	Tabriz (Iran)	Meteorological observations	Model simulation	High building height-to-width ratios improve thermal comfort by shading.
Lau et al. (2019)	Hong Kong (China)	Questionnaire surveys and field measurements	ANOVA	Compact high-rise buildings (LCZ 1) experience the highest air temperatures and strongest heat discomfort.
Kotharkar & Dongarsane (2024)	Nagpur (India)	Model simulation	One-way ANOVA	LCZ 3 and LCZ 9 face extreme daytime thermal stress.
Verdonck et al. (2017)	Brussels, Antwerp and Ghent (Belgium)	Model simulation	Comparison of LCZ temperature differences	Compact mid-rise areas (LCZ 2) are hottest, sparse areas (LCZ 9) coolest, LCZ 6 shows most spatial temperature heterogeneity.
Kotharkar et al. (2024)	Nagpur (India)	Meteorological observations	One-way ANOVA	Large, sparsely built areas (LCZs 8 and 9) face higher heat stress, while vegetated low-rise areas resist.
Rahman et al. (2021)	The university campus in Germany	Field measurements	ANOVA and Tukey HSD test	Urban green spaces reduce HPT, with grass surfaces in wet spells offering greater comfort.
Li et al. (2020)	Hong Kong (China)	Questionnaire surveys and field measurements	Multiple linear regression	Shade from buildings and trees improves thermal comfort, influenced by humidity, wind, and radiation.
Geletić et al. (2018)	Brno (Czech Republic)	Weather station and model simulation	ANOVA and Tukey HSD test	Higher humidity worsens thermal discomfort in vegetated (LCZ 9) and water areas (LCZ G).
Thapa et al. (2024)	Cities in India	Simulation climate data	Map visualization	Thermal comfort and microclimates vary significantly across different regions.

to investigate the spatiotemporal patterns of HPT across different LCZs by taking NCP as an example. By comparing the HPT changes between normal and extreme weather, we also quantitatively evaluate how HPT variations in different LCZs in response to extreme weather. This study aims to enhance our understanding of fine-scale HPT changes in different urban environments under extreme weather conditions, contributing to climate change-related health impact assessments and the development of more resilient urban environments. These findings are crucial for informing policies aligned with the United Nations Sustainable Development Goals (SDGs), particularly SDG 3 (Good Health and Well-being), SDG 11 (Sustainable Cities and Communities), and SDG 13 (Climate Action).

2. Material and methods

2.1. Study area

The NCP area (113°E – 121°E and 34°N – 41°N ; see Fig. 1) is the largest alluvial plain in East Asia, holding >400 million people across eleven provinces of China. This region encompasses densely populated Beijing-Tianjin-Hebei urban agglomeration and megacities such as Zhengzhou and Jinan (Kang & Eltahir, 2018). As one of China's key agricultural hubs, NCP is responsible for over half of the nation's wheat output and nearly one-fifth of the world's maize production (Han et al., 2018; Kendy et al., 2003; National Bureau of Statistics of China, 2022). Located in a subtropical humid climate, NCP experiences strong solar radiation and high precipitation, with summer being both the雨iest and hottest season of the year (Wan et al., 2022; Wei et al., 2019). NCP faces escalating heat stress risks under ongoing climate warming. On

average, over annual 22 million people are exposed to summer extreme heat days in NCP (Wu et al., 2019b; Zhang et al., 2015; Zhao et al., 2019). These challenges are particularly severe in rapidly urbanizing areas with intense population growth such as Beijing, the capital of China (Wang et al., 2022; Xu et al., 2024).

2.2. Datasets

2.2.1. Human thermal index collection

A daily human thermal index collection with a spatial resolution of 1 km, named HiTIC-NCP (Li et al., 2023), was utilized in this study. The HiTIC-NCP dataset has excellent performance, with averaged determination coefficient (R^2), root mean absolute error (MAE), and average root mean squared error (RMSE) values of 0.987, 0.970 °C, and 1.292 °C, respectively, thus can effectively capture day-to-day HPT variabilities. The dataset includes 12 widely-used human thermal indices (see Table 2), including HI, WCT, WBT, etc. The HI index is commonly employed to represent HPT in hot weather, whereas WCT is utilized to quantify the combined effect of wind and low temperatures. So, we adopted HI and WCT only for summer (June to August) and winter (December to February), respectively, among the twelve HPT indices. Using HiTIC-NCP, we explored the relationship between HPT and LCZs, and assessed the HPT differences between extreme temperature days and normal weather days across different LCZs.

2.2.2. Meteorological observations

Daily 2 m minimum air temperature (T_{\min}) observations from 2003 to 2020 were obtained from national meteorological stations in NCP, provided by the China National Climate Center (<http://data.cma.cn>).

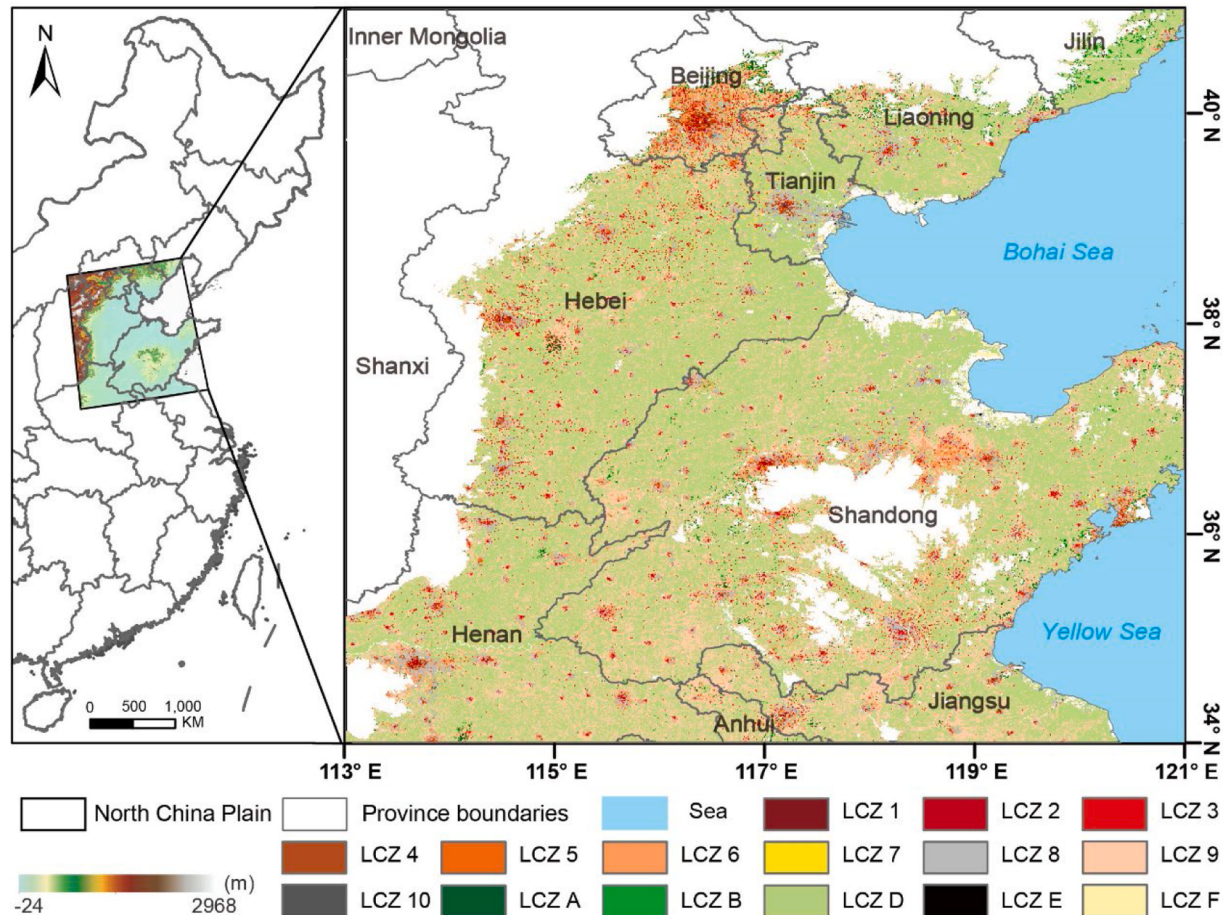


Fig. 1. Topography and administrative divisions of the North China Plain (NCP) and spatial distribution of LCZs in the areas with elevation within 200 m in NCP. The blank areas in the right subplot are water bodies and land areas with elevations exceeding 200 m.

Table 2
Human thermal indices in HiTIC-NCP.

Abbreviation	Human Thermal Index	Computation Equations	Reference
ATin	Apparent Temperature (indoors)	$AT_{in} = -1.3 + 0.92 \times T + 2.2 \times E_a$	(Steadman, 1979)
AT _{out}	Apparent Temperature (outdoors, in the shade)	$AT_{out} = -2.7 + 1.04 \times T + 2 \times E_a - 0.65 \times V$	(Steadman, 1984)
DI	Discomfort Index	$DI = 0.5 \times WBT + 0.5 \times T$	(Epstein & Moran, 2006)
ET	Effective Temperature	$ET = T - 0.4 \times (T - 10) \times (1 - 0.001 \times RH)$	Gagge et al. (1971)
NET	Net Effective Temperature	$NET = 37 - \frac{37 - T}{0.68 - 0.0014 \times RH + \frac{1}{1.76 + 1.4 \times V^{0.75}}}$	Houghton et al. (1923)
HMI	Humidex	$HMI = T + 0.5555 \times (0.1 \times E_a - 10)$	Masterton & Richardson (1979)
MDI	Modified Discomfort Index	$MDI = 0.75 \times WBT + 0.38 \times T$	(Moran et al., 1998)
SAT	Surface Air Temperature	Air temperature at 2-meter height	/
sWBGT	Simplified Wet-bulb Temperature	$sWBGT = 0.567 \times T + 0.0393 \times E_a + 3.94$	Willett & Sherwood (2012)
WBT	Wet-bulb Temperature	$WBT = T \times \text{atan}(0.151977 \times (RH + 8.313659)^{0.5}) + \text{atan}(T + RH) - \text{atan}(RH - 1.676331) + 0.00391838 \times RH^{1.5} \times \text{atan}(0.02301 \times RH) - 4.686035$	Stull (2011)
HI	Heat Index	$HI^* = -8.784695 + 1.61139411 \times T - 2.338549 \times RH - 0.14611605 \times T \times RH - 1.2308094 \times 10^{-2} \times T^2 - 1.6424828 \times 10^{-2} \times RH^2 + 2.211732 \times 10^{-3} \times T^2 \times RH + 7.2546 \times 10^{-4} \times T \times RH^2 + 3.582 \times 10^{-6} \times T^2 \times RH^2$	(Rothfusz & Headquarters, 1990)
WCT	Wind Chill Temperature	$WCT = 13.12 + 0.6215 \times T - 11.37 \times (V \times 3.6)^{0.16} + 0.3965 \times T \times (V \times 3.6)^{0.16}$	Osczevski & Bluestein (2005)

T is air temperature ($^{\circ}\text{C}$) at 2-meter height, RH is relative humidity (%), V is wind speed (m/s). E_a is actual vapor pressure (kPa), and is calculated by $E_a = \frac{RH}{100} \times 6.112 \times e^{\left(\frac{17.67 \times T}{T+243.5}\right)}$. The asterisk (*) means that an adjustment is needed (NOAA, https://www.wpc.ncep.noaa.gov/html/heatindex_equation.shtml). The unit of all human thermal indices is degree Celsius ($^{\circ}\text{C}$).

We selected 81 weather stations within the built-up areas of the cities in NCP and identified extreme temperature days (i.e., extreme heat and extreme cold) for each city (refer to [Section 2.3.1](#)) based on meteorological records.

2.2.3. Auxiliary datasets

We used digital elevation model (DEM) data, LCZ map, MODIS land cover type, and China cities built-up area dataset as auxiliary datasets (see [Table 3](#)). All gridded datasets were re-gridded to 1 km resolution for consistency. The detailed data are described as follows. Altitude can influence regional temperature ([Gao et al., 2024](#); [You et al., 2020](#)). The highest elevation in NCP reaches nearly 3000 m, while the area with low elevations (i.e., ≤ 200 m) accounts for 67 % of the whole region. Using the Multi-Error-Removed Improved-Terrain Digital Elevation Model (MERIT-DEM) ([Yamazaki et al., 2017](#)), we extracted the flat areas with elevations ≤ 200 m, covering most urbanized and populated areas, for further investigation.

The 2018 global 100 m resolution LCZ map generated by [Demuzere et al. \(2022\)](#) was utilized. This map captures the intra-urban heterogeneity and characterizes detailed urban landscapes ([Stewart & Oke, 2012](#)), classifying the NCP region into 10 urban built-up categories (i.e., LCZs 1~10) and 7 natural areas (i.e., LCZs A~G) ([Bechtel & Daneke, 2012](#)). Built-up LCZ categories, such as LCZs 1~6, exhibit significant variations in height and density, as detailed in [Table 4](#). LCZs 1~3 (i.e., high-, mid-, or low-rise buildings, respectively) are formatted as compact agglomerations individually, whereas LCZs 4~6 are various height buildings with a sparse arrangement. LCZs A~D indicate natural land cover types with different heights of vegetation. We resample LCZ map into a spatial resolution of 1 km. LCZ C (i.e., shrubs and bushes) and LCZ G (i.e., water) are excluded.

LCZs 1~10) and 7 natural areas (i.e., LCZs A~G) ([Bechtel & Daneke, 2012](#)). Built-up LCZ categories, such as LCZs 1~6, exhibit significant variations in height and density, as detailed in [Table 4](#). LCZs 1~3 (i.e., high-, mid-, or low-rise buildings, respectively) are formatted as compact agglomerations individually, whereas LCZs 4~6 are various height buildings with a sparse arrangement. LCZs A~D indicate natural land cover types with different heights of vegetation. We resample LCZ map into a spatial resolution of 1 km. LCZ C (i.e., shrubs and bushes) and LCZ G (i.e., water) are excluded.

Cropland is an essential component of NCP and plays a pivotal role in regulating local humidity, temperature, etc. ([Mishra et al., 2020](#); [Zhang et al., 2019](#)). We utilized the MODIS land cover type product (MCD12Q1) coupled with the International Geosphere-Biosphere Program (IGBP) classification system to identify cropland areas within NCP. This dataset has a spatial resolution of 500 m, and marks grids with >60 % of the cultivated land area as cropland. According to the definitions and descriptions of each classification in LCZs and MCD12Q1-IGBP data, we extract cropland areas from the LCZ 9 and LCZ D areas of NCP.

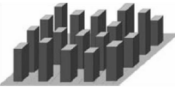
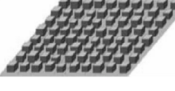
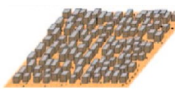
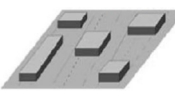
The China built-up area dataset produced by [Jiang et al. \(2022a\)](#), with an average overall accuracy of 95.57 % and a kappa coefficient of 0.91, is employed to select weather stations that are used to identify extreme temperature days. This dataset includes individual built-up regions in 433 Chinese cities with populations $>300,000$, of which 48 cities are in NCP. For each city in NCP, we construct the minimum circumscribed convex shape of the city built-up area to capture the geometric shape characteristics of the urban area and expanded a buffer zone with the same area as the built-up area outwards from the city boundaries ([Zhang et al., 2022a](#)). The buffer zone includes sufficient natural surface area for subsequent analysis concerning local-scale HPT and LCZs under temperature extremes (refer to [Section 3.2](#)).

Table 3
Auxiliary datasets used in this study.

Dataset	Spatial Resolution	Temporal Resolution	Time	Reference
DEM	~100 m	/	/	Yamazaki et al. (2017)
LCZ map	Aggregated to 1 km	Annual	2018	Demuzere et al. (2022)
MODIS land cover type (croplands)	Aggregated to 1 km	Annual	2018	Friedl & Sulla-Menashe (2022)
China cities built-up area	Aggregated to 1 km	Annual	2020	Jiang et al. (2022a)

Table 4

Local climate zones analyzed in this study (modified from [Stewart and Oke \(2012\)](#)).

LCZ Types	Graphic	Description
LCZ 1 (Compact high-rise)		Dense high-rise buildings (>10 floors) with little greenery. Characterized by high coverage, tall structures, and limited open space.
LCZ 2 (Compact mid-rise)		Dense mid-rise buildings (3~9), moderate greenery, and paved surfaces. Compact structure with few open spaces.
LCZ 3 (Compact low-rise)		Dense low-rise buildings (1~3), minimal vegetation. Primarily residential with small spaces between buildings.
LCZ 4 (Open high-rise)		High-rise buildings (>10) with significant open spaces and moderate greenery. Less compact compared to LCZ 1.
LCZ 5 (Open mid-rise)		Mid-rise buildings (3~9) surrounded by open areas. Moderate density with residential, commercial, or mixed use.
LCZ 6 (Open low-rise)		Low-rise buildings (1~3), substantial open space and greenery. Primarily suburban or rural residential settings.
LCZ 7 (Lightweight low-rise)		Low-rise buildings (1~3) with lightweight materials. Typically found in informal settlements or areas with lower building standards.
LCZ 8 (Large low-rise)		Single-floor buildings with large footprints, such as warehouses or industrial complexes, often with large open areas.
LCZ 9 (Sparsely built)		Scattered small buildings, separated by large open or vegetated areas.
LCZ 10 (Heavy industry)		Factories, industrial buildings with large footprints, significant impervious surfaces, and little vegetation.
LCZ A (Dense trees area)		Areas densely covered with trees, resembling natural forests or urban parks with high tree coverage.
LCZ B (Scattered trees area)		Areas with scattered trees interspersed with grass or bare soil. Often found in suburban or rural areas.
LCZ D (Low plants area)		Areas primarily covered with grass, shrubs, or other low vegetation.
LCZ E (Bare rock/paved area)		Hard surfaces without vegetation, such as rocks, paved areas, or construction sites. High thermal conductivity and low albedo.
LCZ F (Bare soil/sand area)		Areas covered with bare soil, loose sand, or other unconsolidated materials. Found in desert environments or construction zones.

2.3. Methods

2.3.1. Definition of temperature extremes

Extreme temperature events are determined based on daily T_{\min} records ([Luo et al., 2022](#)). Previous studies have demonstrated that daily T_{\min} is susceptible to warming due to consecutive hot days, and nights without heat relief from high temperatures can pose a severe threat to public health ([Lin et al., 2018](#); [Meehl & Tebaldi, 2004](#)). For each city, extreme heat (cold) days are defined when station-based daily T_{\min} is significantly warmer (colder) than local and season-varying 90th percentile, which is calculated by ordering the 15-day series (i.e., seven days prior and subsequent) encompassing a calendar day (i.e., day of year, DOY) within the reference period spanning from 2003 to 2020 ([Cheng et al., 2023](#); [Dong et al., 2024](#)). Using other temperature indicators (e.g., daily maximum or mean temperatures) yield similar results (not shown).

2.3.2. Quantitative comparison of HPT changes

The variations in HPT under extreme temperature events are defined as the difference in HPT between extreme and normal weather, that is, mean HPT under extreme weather minus that on normal days ([Roshan et al., 2024](#); [Wang et al., 2019a](#)). The impacts of LCZs on HPT during extreme temperature events are assessed in two phases. First, a corrected one-way Welch's analysis of variance (ANOVA) for multiple groups with unequal variances ([Welch, 1951](#)) exerts to examine the statistical significance of the disparities in HPT changes among various LCZs ([Zhao et al., 2020](#)). Second, if significant differences exist in at least one pair of LCZs, we further compare the HPT changes between different LCZs under extreme weather conditions using the Games-Howell method ([Games & Howell, 1976](#)), which was designed to compare multiple groups more robustly, allowing for unequal variances and sample sizes. The degrees of freedom for Welch's ANOVA are calculated using the Welch-Satterthwaite formula, which incorporates group sample sizes and variances ([Karim et al., 2023](#)). Similarly, the Games-Howell method computes the degrees of freedom based on the sample sizes and variances of each group. The Games-Howell method enables the determination of whether there are significant differences between the two types of LCZs pair-wise, and quantitatively evaluates the differences between the groups. Welch's ANOVA and Games-Howell algorithm were implemented with the R-package "rstatix". We provide a technical roadmap outlining the research tools, methodological steps, and analysis framework applied in this study ([Fig. 2](#)).

3. Results and analysis

3.1. Mean HPT in relation to LCZs

The summer mean of daily HPT in LCZs over the area with elevation <200 m from 2003 to 2020 is displayed in [Fig. 3](#). The average HPTs in built-up areas (i.e., LCZs 1~10) are warmer than those in natural types (i.e., LCZs A~F) and cropland. The average summer HIs for the built-up region, natural area, and cropland are 27.69 °C, 27.26 °C, and 27.09 °C, respectively. Impervious covers and built environments alter the underlying surface in the region and contribute to increased local summer HPT relative to natural landscapes.

Urban forms (e.g., building density and height) have impacts on human thermal environment by influencing regional energy budget. Among LCZs, building heights gradually decrease from LCZs 1 to 3 (compact zones) and from LCZs 4 to 6 (open zones). Correspondingly, the average HPT decreases from 28.67 °C in LCZ 1 (compact high-rise buildings) to 27.86 °C in LCZ 3 (compact low-rise buildings) and from 28.23 °C in LCZ 4 (open high-rise buildings) to 27.48 °C in LCZ 6 (open low-rise buildings), as shown in [Fig. 3k](#). Greater building height correlates with increased impervious surface area and lower albedo, leading to a larger absorption of solar radiation and higher HPTs in mid- and high-rise buildings than low-rise buildings ([Du et al., 2024](#); [Jiang et al., 2024](#)).

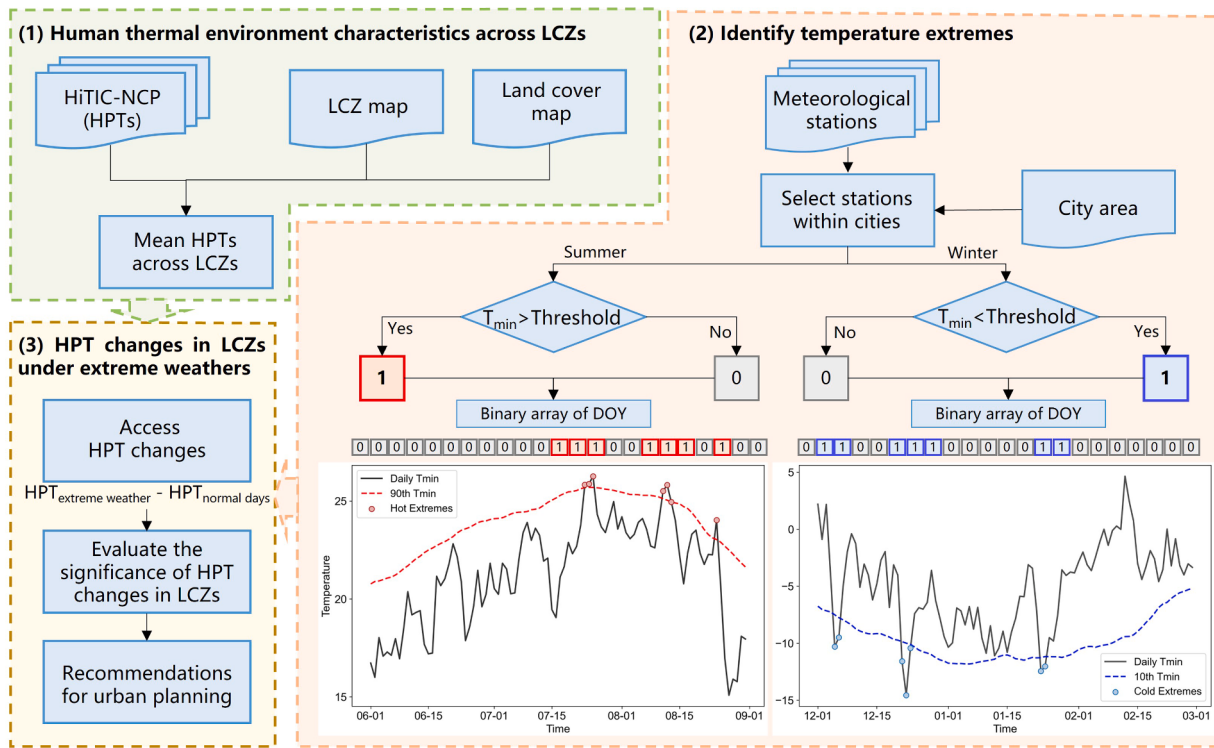


Fig. 2. The framework in this study.

2022b). This effect is more pronounced in densely built areas, as reflected in the HPT difference of 0.81°C between LCZ 1 and LCZ 3, compared with a smaller difference of 0.75°C between LCZ 4 and LCZ 6 in open clusters. This result underscores how compact areas experience a stronger impact of building density on summer HPT. Densely packed buildings restrict heat dissipation and intensify the urban heat island (UHI) effect (Shen et al., 2024; Tian et al., 2019), resulting in higher HPTs than those found in open-structure building clusters. In addition, large construction materials (i.e., LCZ 8 with concrete or stone material, 27.85°C) and factory clusters with heat-generating activities (i.e., LCZ 10, 27.70°C) result in relatively high summer HPT in the local region. Among natural LCZs, HPT in LCZ E (27.72°C) is similar to the mean HPT in built-up areas (27.69°C), and the average HPT values decrease with increasing vegetation cover, which is evident from higher HPT in LCZ F (27.43°C) compared with LCZ D (27.17°C), LCZ A and LCZ B (average of 25.85°C). Among all LCZ types, tree-covered areas exhibit the lowest summer HPT, aligning with the findings of Turner et al. (2023) and Rahman et al. (2022). Tree-covered areas are influenced by factors such as tree canopy shade and transpiration effects, thereby reducing summer HPT, thus effectively mitigating the threat of summer heat stress for urban residents. However, tree density has complex consequences on HPT. Areas with dense trees tend to have higher HPT than the areas with sparse trees, with the average summer HPT for dense tree areas (i.e., LCZ A) and sparse tree areas (i.e., LCZ B) being 26.13°C and 25.85°C , respectively.

Summer HPT indices across different LCZs of NCP have increased from 2003 to 2020 (Fig. 4). The most pronounced warming trend of HPT is observed in LCZ 10, at a rate of 0.82°C per decade, while tree-covered areas exhibit the slowest rate of HPT increase. The HPT warming trend intensifies as building height decreases, with a clear gradient increase from high-rise buildings (e.g., LCZ 1) to low-rise buildings (e.g., LCZ 3). Moreover, low-rise building areas (i.e., LCZ 3, and LCZs 6~10) display a stronger warming trend, with the growth rate of HI exceeding 1°C per decade.

The pattern of winter HPT in various LCZs differs from that in summer. Built-up areas show the warmest winter HPT (-2.19°C) in NCP.

However, due to the impact of winter agricultural crop growth on local climate, HPT in cropland is higher than in natural surface areas, with the winter average WCT being -2.49°C for cropland and -3.02°C for natural surfaces (Fig. 5). A similar phenomenon has also been observed in previous studies, which noted that winter agriculture increases cropland temperatures due to winter cultivation and enhanced crop evapotranspiration (Wang et al., 2013; Wu et al., 2019a). Compact mid-rise building areas (i.e., LCZ 2) demonstrate a favorable thermostatic effect in winter and have the highest winter HPT (-0.93°C) among all LCZs. LCZ 7 (-3.74°C) shows the lowest winter HPT among built-up LCZs, and LCZ E (-3.71°C) has the lowest value among natural LCZs. They are attributed to their light building material with low thermal capacity in LCZ 7 and featureless landscape of rock with low albedo and limited absorption of solar radiation in LCZ E, making them typically colder than other regions in winter. Tree-covered areas have an average winter WCT of -3.77°C , and exhibit the lowest values in AT_{out}, NET, and WCT among natural LCZs.

The long-term trends of winter HPT since 2003 across different LCZs are examined in Fig. 6. Most HPT indices in non-tree-covered LCZs exhibit an increasing trend, particularly NET and WCT. The warming trend in built-up areas is more pronounced than in natural surfaces, indicating that impervious cover has a warming effect on elevated winter HPT. Denser building structure further amplifies the warming trend in winter HPT. LCZ 10 exhibits the highest rising trend among all LCZs, while areas with sparse trees show a significant decrease in NET by -0.90°C per decade.

3.2. HPT changes under extreme weather conditions

The HPT changes during extreme heat events in various LCZs of metropolitan areas in NCP from 2003 to 2020 are shown in Figs. 7 and 8. All HPT indices in various LCZs exhibit similar patterns. During hot events, the underlying surfaces in the region receive more solar radiation, posing an elevated heat risk in all LCZs. The largest HPT increase under hot weather is observed in natural surfaces, followed by cropland and built-up regions. LCZ 7 constructed by building material with high

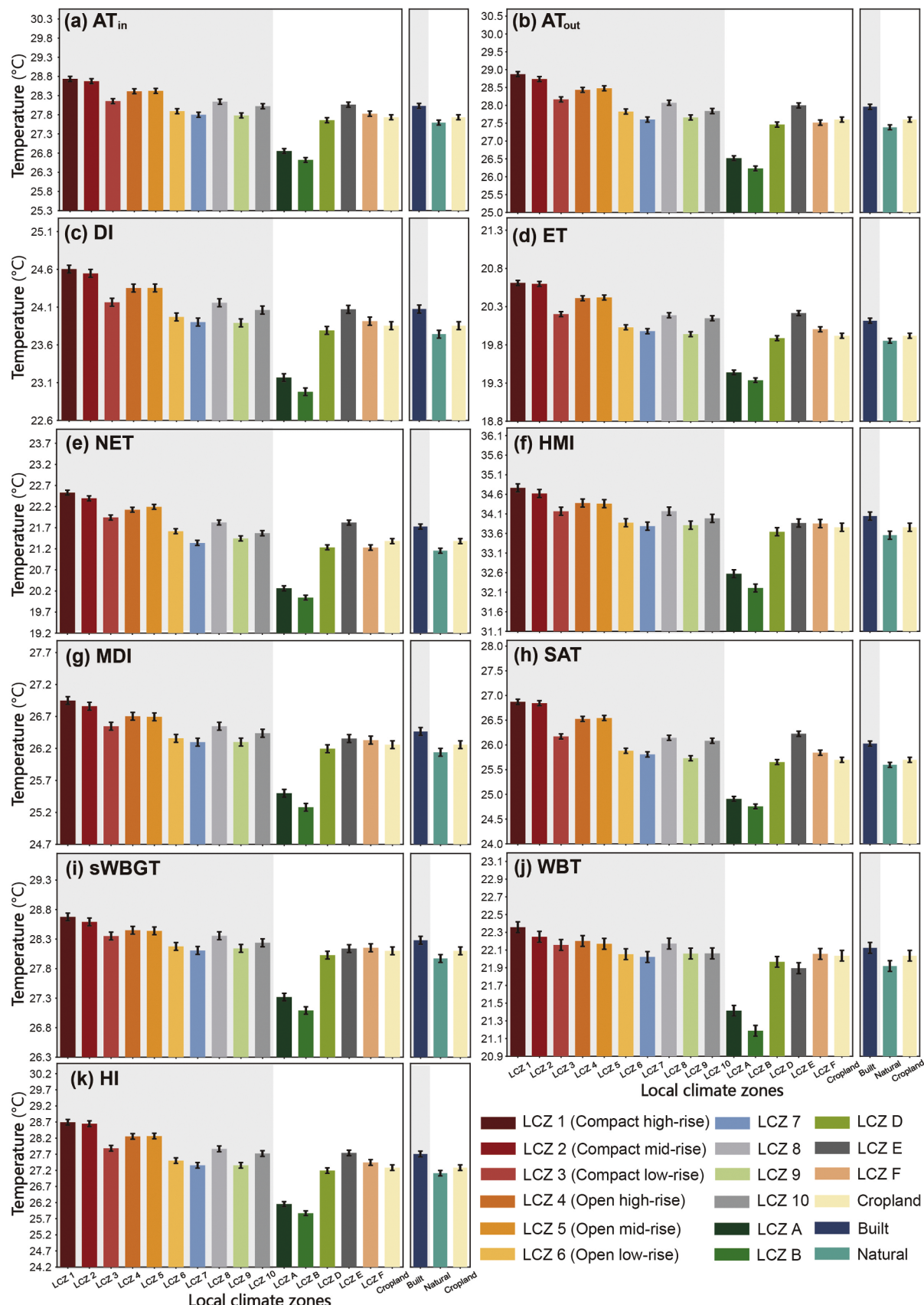


Fig. 3. Summer mean HPT in different LCZs of NCP: (a) AT_{in} , (b) AT_{out} , (c) DI, (d) ET, (e) NET, (f) HMI, (g) MDI, (h) SAT, (i) sWBGT, (j) WBT, and (k) HI. The light gray background indicates HPT in built-up LCZs, and the white background indicates natural and cropland regions. HPT in different LCZs and cropland are shown in the bar plot on the left side. The LCZs are categorized into three main types (i.e., built area, natural land, and cropland), the HPT of which are shown on the right side. Error bars represent mean \pm standard error.

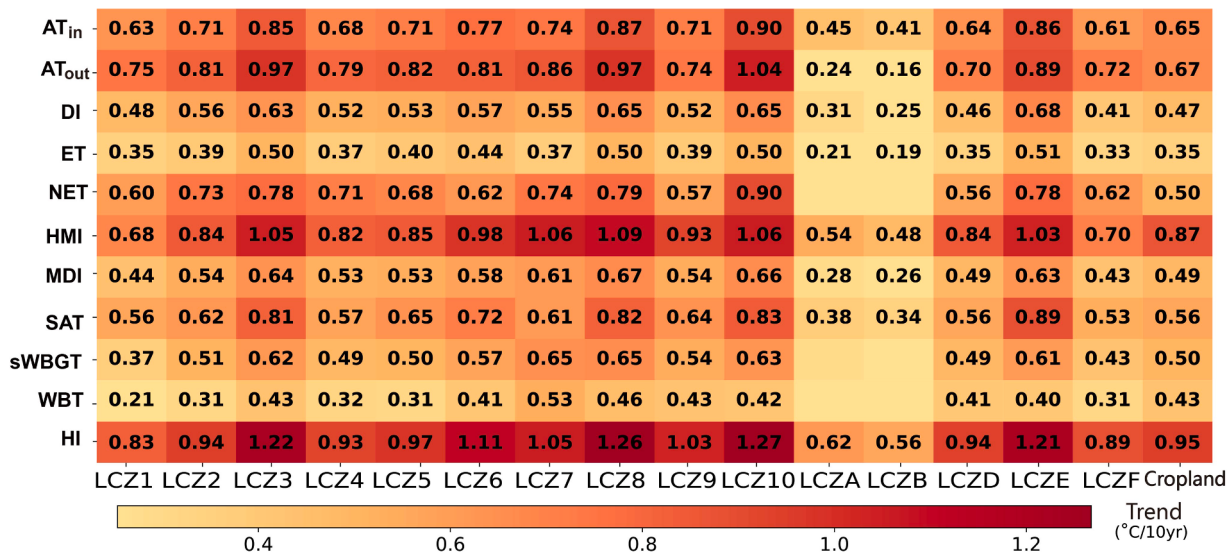


Fig. 4. Temporal trends of summer human thermal indices in various LCZs of NCP from 2003 to 2020. The number indicates a significant linear trend (unit: per decade) of HPT in each LCZ at the 0.05 level, while blank cells indicate non-significant trends.

thermal conductivity, heats up quickly under extreme heat, experiencing the largest HPT increase among LCZs with an HI change of 4.88 °C. LCZ 10, where the high proportion of impervious surfaces enhances the heat storage in extreme heat and often concentrates anthropogenic heat emissions from the environment, is the second one, showing an HI increase of 4.59 °C. Owing to the lack of vegetation to help regulate heat fluxes (Ma et al., 2023; Zhou et al., 2022), LCZ F comprised almost entirely bare soil or sands has the largest HI change (4.60 °C) among natural surfaces. LCZs 7, 10, and F are more vulnerable to high temperatures than other LCZs. The lowest HPT variations are observed in tree-covered areas, demonstrating that urban trees serve a critical role in heat mitigation through increased transpiration efficiency and shading effect (Zhou et al., 2017). This results in a large reduction in heat differentials, with HPT changes of 3.55 °C in dense tree areas and 3.64 °C in sparse tree areas.

Urban morphology and geometry influence the energy balance in a complex manner (Lin et al., 2017). Received solar radiation elevates as height grows. However, the increase in building height not only advances regional surface roughness, promoting convective heat dissipation in the region, but also provides building shade for residents to avoid direct sunlight. When extreme heat event occurs, the change in solar radiation absorption in shaded areas is smaller than that in areas without shade, thus resulting in moderate HPT increases in high- and mid-rise building areas. Due to their higher solar radiation absorption (Du et al., 2024), high-rise building areas still suffer from a larger HPT increase in extreme heat than mid-rise buildings do. The open arrangement of buildings will further promote the absorption of solar radiation and allow the quicker dissemination of long-wave radiation to the adjacent regions, showing more pronounced warming than compact building areas. For example, the HI increases during extreme heat days in high-rise (LCZ 1), low-rise (LCZ 3), and mid-rise areas (LCZ 2) are 4.03 °C, 4.10 °C, and 3.85 °C, respectively. The HI increase in open mid-rise areas (i.e., LCZ 5, 4.04 °C) is greater than in LCZ 2.

Areas with compact mid-rise buildings (i.e., LCZ 2) experience a high summer HPT, posing a severe thermal risk to urban residents. However, the HPT increases during extreme heat events are the smallest in LCZ 2, which is likely due to the shading effect of urban buildings. LCZs 7 and 10 experience particularly severe human-perceived heat stress during extreme heat days due to high thermal conductivity and increased heat storage of the impervious surfaces. These areas present significantly stronger HPT increases than other LCZ types across 12 HPT indices. For instance, the HI increase in LCZ 7 is significantly higher than other LCZs,

ranging from 0.28 °C to 1.33 °C. Trees exert an essential role in mitigating urban heat through increased evapotranspiration efficiency and shading effect during extreme heat, exhibiting a remarkable cooling effect. Trees-covered areas undergo moderate increases in most HPT indices, but WBT and sWBGT in trees-covered areas exhibit greater warming changes during extreme heat than in mid- and high-rise building areas (i.e., LCZs 1, 2, 4, and 5). This phenomenon may be attributed to artificial irrigation for trees during summertime months or the enhanced evapotranspiration of trees in response to rising temperatures during extreme heat. It not only contributes to reducing local temperature but also increases humidity, and the latter can worsen human heat stress during extreme hot conditions (Wang et al., 2019a). Additionally, cropland in NCP experiences an obvious HPT increase during hot episodes, which is significantly higher than in most residential areas (i.e., LCZs 1 to 6) and tree areas.

Drops in 12 HPT indicators during extreme cold events in the winter season and their disparities across different LCZs are shown in Figs. 9 and 10. These HPT changes exhibit similar patterns among various LCZs, which are different from those in summer. Croplands exhibit a stronger HPT drop during cold events than built-up surfaces do. Areas with trees experience greater HPT decreases than other types across for almost all HPT indices, particularly for NET and WCT. Among built-up areas, LCZs 2 and 3, where buildings are constructed compactly, exhibit weak heat dissipation and less variation in outgoing long-wave radiation under cold weather. These areas demonstrate desirable thermostatic effects with smaller HPT decreases than other LCZs. Compared with other LCZs, LCZs 7 and 10 show remarkably stronger HPT decreases when cold events occur, with winter HI differences of -6.14 °C and -6.11 °C, respectively. Intense HPT changes under cold weather are similar to those under hot conditions, demonstrating the limited capacity of these two LCZ types to cope with extreme temperature events and their vulnerability to temperature extremes.

4. Discussion

4.1. Inter-LCZs thermal characteristics of the land surface temperatures

Land surface temperature (LST) describes a thermal state resulting from changes in the earth's surface and its interaction with the atmosphere, and is also crucial in understanding the heat energy balance and regional thermal flux (Geng et al., 2023; Hou et al., 2023). Here we adopt a seamless daily LST dataset (i.e., MODIS-like LST) (Zhang et al.,

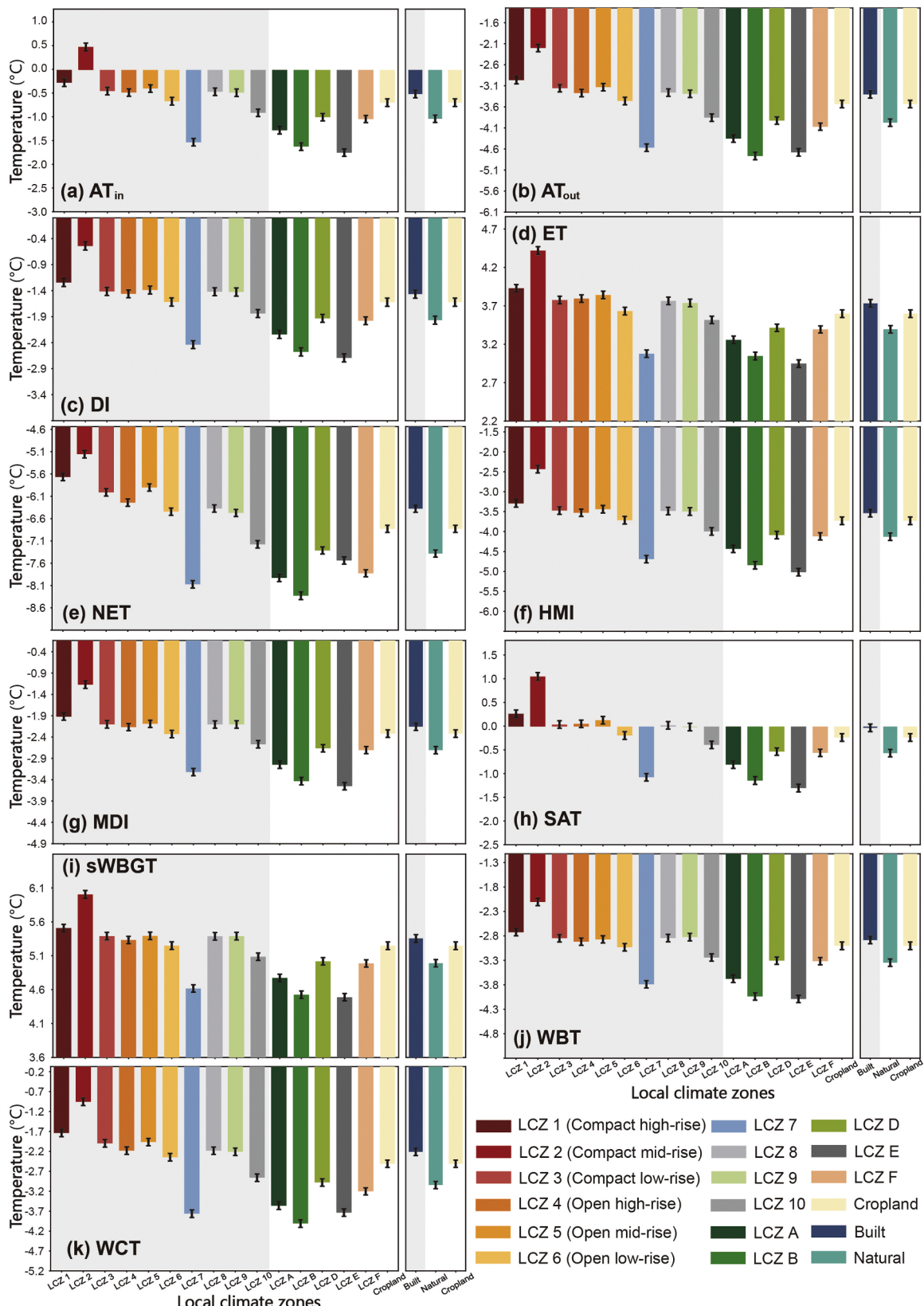


Fig. 5. Winter mean HPT in different LCZs of NCP: (a) AT_{in} , (b) AT_{out} , (c) DI, (d) ET, (e) NET, (f) HMI, (g) MDI, (h) SAT, (i) sWBGT, (j) WBT, and (k) WCT. The light gray background indicates HPT in built-up LCZs, and the white background indicates natural and cropland regions. HPT in different LCZs and cropland are shown in the bar plot on the left side. The LCZs are categorized into three main types (i.e., built area, natural land, and cropland), the HPT of which are shown on the right side. Error bars represent mean \pm standard error.

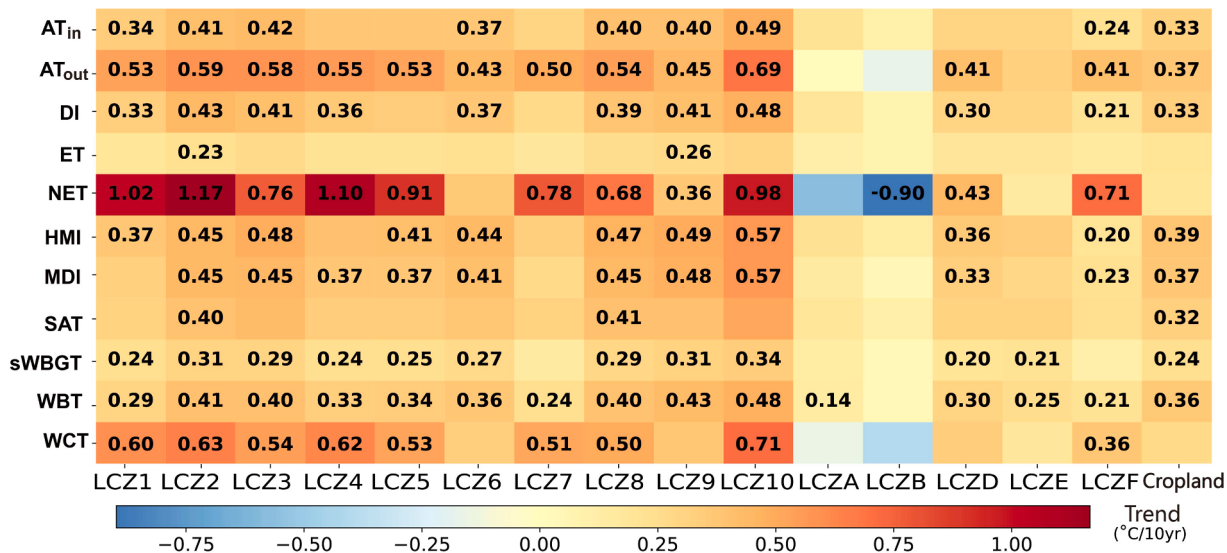


Fig. 6. Temporal trends of winter human thermal indices in various LCZs of NCP from 2003 to 2020. The number indicates a significant linear trend (unit: per decade) of HPT in each LCZ at the 0.05 level, while blank cells indicate non-significant trends.

2022b) to evaluate the thermal characteristics of LCZs in terms of LST, and further elucidate the possible mechanisms through a comparative analysis of how various LCZs affect HPT and LST. As shown in Fig. 11a, the summer LST patterns in different LCZs are overall similar to the HPT pattern. The increase in impervious surfaces alters regional energy balance by enhancing solar radiation absorption and increasing sensible heat within the area, leading to a significantly higher LST in built-up areas (26.55°C) compared with cropland (25.24°C) and natural surfaces (25.09°C). LSTs in mid- to high-rise building areas are higher than in low-rise areas and further intensify with increasing building density. However, the impact of various urban elements (such as building height) on LST is generally stronger than that on HPT. In addition, tree density has a greater impact on HPT than on LST. For example, HI in LCZ A is 26.13°C , which is higher than in LCZ B (25.85°C), while the LSTs are 23.86°C and 23.90°C in LCZs A and B, respectively. In winter, built-up areas have the highest LST of -0.12°C , while natural surfaces have the lowest LST of -1.04°C (Fig. 11b). LCZ 2 has the highest LST and HPT among all LCZs, while tree-covered areas have the lowest winter surface temperatures, i.e., -1.63°C in LCZ A and -2.09°C in LCZ B.

The LST increases during extreme heat weather across different LCZs and their differences are shown in Fig. 11c and Fig. 11e. The LST increase in built-up areas (1.91°C) is higher than that in natural surfaces (1.89°C), which is distinct from the HPT change, where natural surfaces exhibit a greater increase. LCZ 10 (2.06°C) and LCZ E (1.98°C) experience the largest LST increases under hot weather in built-up and natural LCZs, respectively. Low-rise building areas (i.e., LCZs 3 and 6), with their high sky view factor and extensive impervious surface exposure, absorb more shortwave solar radiation, leading to a significant LST increase under hot weather, which is greater than that in high- and mid-rise building areas. Tree-covered areas exhibit the smallest LST increase during heat events (1.72°C), and tree density seems to have a marginal impact on LST changes.

Figs. 11d and 11f display the LST decreases during extreme cold days in winter and their differences among various LCZs. Unlike HPT, the LST decrease in built-up areas (-3.65°C) is greater than that in natural surfaces (-3.54°C). Among all built-up LCZs, LCZ 1 with large impervious surface areas shows the largest LST drop (-3.77°C) under cold weather. Among open-structure building areas, the reduction in LST lessens as the building height decreases, showing that the LST drops in LCZs 4 to 6 during extreme cold episodes are -3.71°C , -3.76°C , and -3.77°C , respectively. During extreme cold weather, tree-covered areas experience a significant LST decrease, which is more pronounced than in

other LCZs. The magnitude of the LST decreases during cold events and intensifies with tree intensity. Different from significant HPT changes in LCZ 7 (-3.71°C) and LCZ 10 (-3.76°C), the LST changes during extreme temperature events in these regions are not observed.

4.2. Limitations and outlook

This study has several limitations that should be noted. Firstly, we analyzed the thermal characteristics of HPT across LCZ categories in NCP using LCZ data in a single year (i.e., 2018). While the 2018 LCZ map provides high-resolution and consistent global coverage, it may not sufficiently represent the dynamic changes in land cover and land use over the past 18 years. Incorporating multi-year land cover/LCZ maps and urban morphology data, such as 3D building heights, would provide a more comprehensive analysis of HPT changes across different LCZs in future research. While we have provided qualitative explanations for differences in HPT under normal and extreme conditions, focusing on building arrangements and shading effects, we did not quantify the contributions of factors such as humidity, wind speed, and elevation. Future research could use mesoscale models (e.g., Weather Research and Forecasting (WRF) model) to simulate and quantify their contributions. Lastly, a broader investigation that includes global-scale assessments of HPT in various LCZs under different climatic backgrounds could help determine whether urban forms have consistent impacts on thermal comfort across diverse environmental settings.

5. Conclusions

In this study, we investigate the human thermal environment variations by quantifying the HPT changes across various LCZs by taking NCP as an example, and further evaluating their response to extreme weather conditions. We find that built-up areas exhibit the highest HPT in both summer (an average HI of 27.69°C) and winter (an average WCT of -2.19°C). Summer HPT increases as building height and density grow, with HI in high-rise areas (averaging for LCZs 1 and 4) reaching 28.45°C , and height differences resulting in a maximum HI difference of 0.81°C (averaging for LCZs 1 and 3). In contrast, areas with tree cover, such as LCZs A and B, exhibit a lower mean HI of 25.85°C , indicating the effectiveness of tree planting in reducing HPT. In winter, compact mid-rise building zones, which have an average WCT of -0.93°C , have the highest HPT in all LCZs, demonstrating their excellent thermostatic effects; whereas, lightweight low-rise building zones (WCT of -3.74°C)

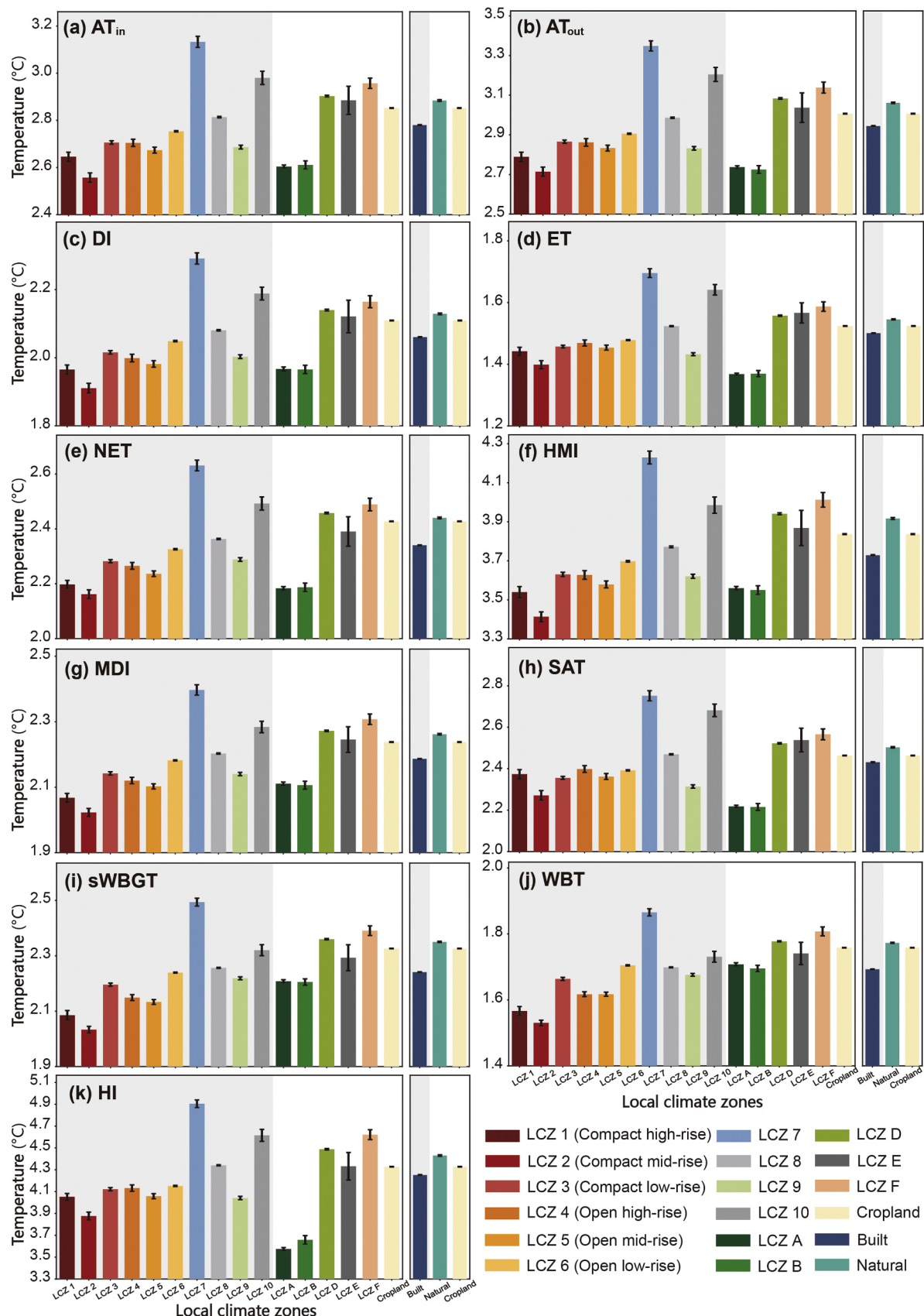


Fig. 7. Summer HPT increases during summer extreme heat events in various LCZs in the metropolitan areas of NCP from 2003 to 2020: (a) AT_{in}, (b) AT_{out}, (c) DI, (d) ET, (e) NET, (f) HMI, (g) MDI, (h) SAT, (i) sWBGT, (j) WBT, and (k) HI. The light gray background indicates HPT in built-up LCZs, and the white background indicates natural and cropland regions. HPT in different LCZs and cropland are shown in the bar plot on the left side. The LCZs are categorized into three main types (i.e., built area, natural land, and cropland), the HPT of which are shown on the right side.

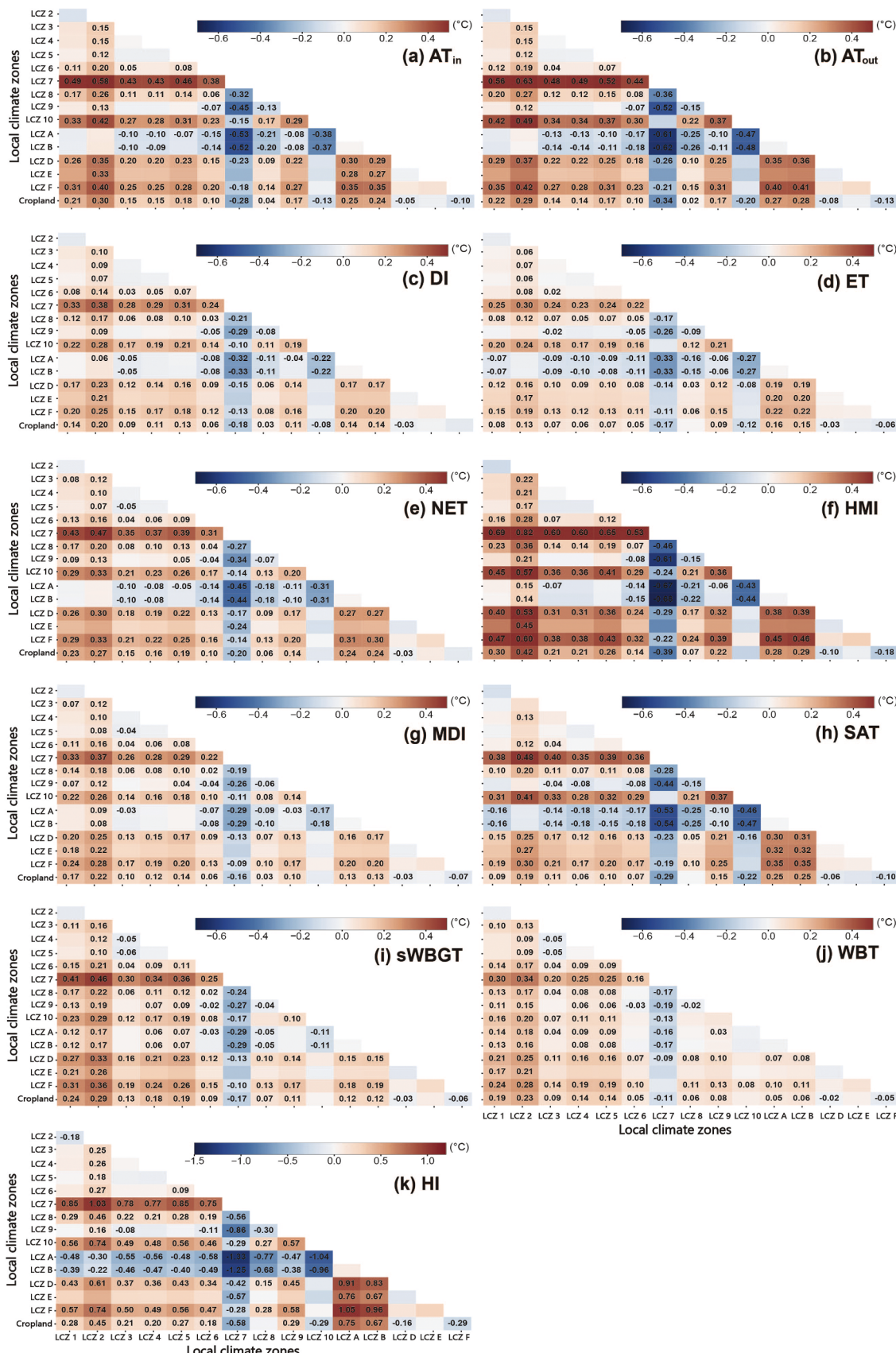


Fig. 8. Differences in the HPT changes under summertime extreme heat weather across various LCZs in the urban areas of NCP from 2003 to 2020: (a) AT_{in} , (b) AT_{out} , (c) DI, (d) ET, (e) NET, (f) HMI, (g) MDI, (h) SAT, (i) sWGBT, (j) WBT, and (k) HI. Black bolded values indicate a significant difference between the two types (i.e., the HPT change in one type in the row minus that in another one in the column) at the 0.05 level. For example, "0.15" in (a) means that the AT_{in} change in LCZ 3 during extreme heat events is significantly higher than that in LCZ 2 by 0.15°C .

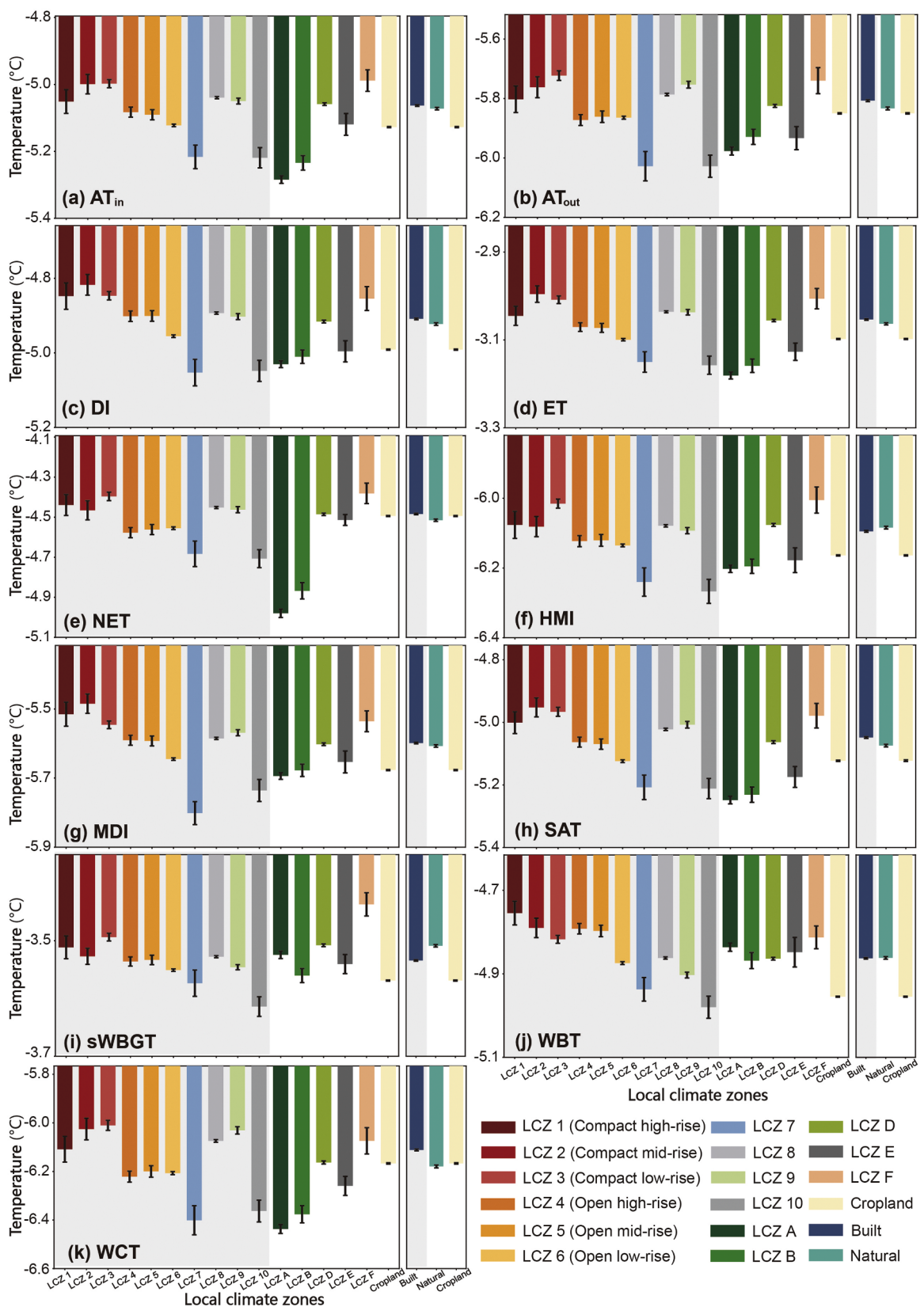


Fig. 9. HPT changes during winter extreme cold events in various LCZs in the metropolitan areas of NCP from 2003 to 2020: (a) AT_{in} , (b) AT_{out} , (c) DI, (d) ET, (e) NET, (f) HMI, (g) MDI, (h) SAT, (i) sWBGT, (j) WBT, and (k) WCT. The light gray background indicates HPT in built-up LCZs, and the white background indicates natural and cropland regions. HPT in different LCZs and cropland are shown in the bar plot on the left side. The LCZs are categorized into three main types (i.e., built area, natural land, and cropland), the HPT of which are shown on the right side.

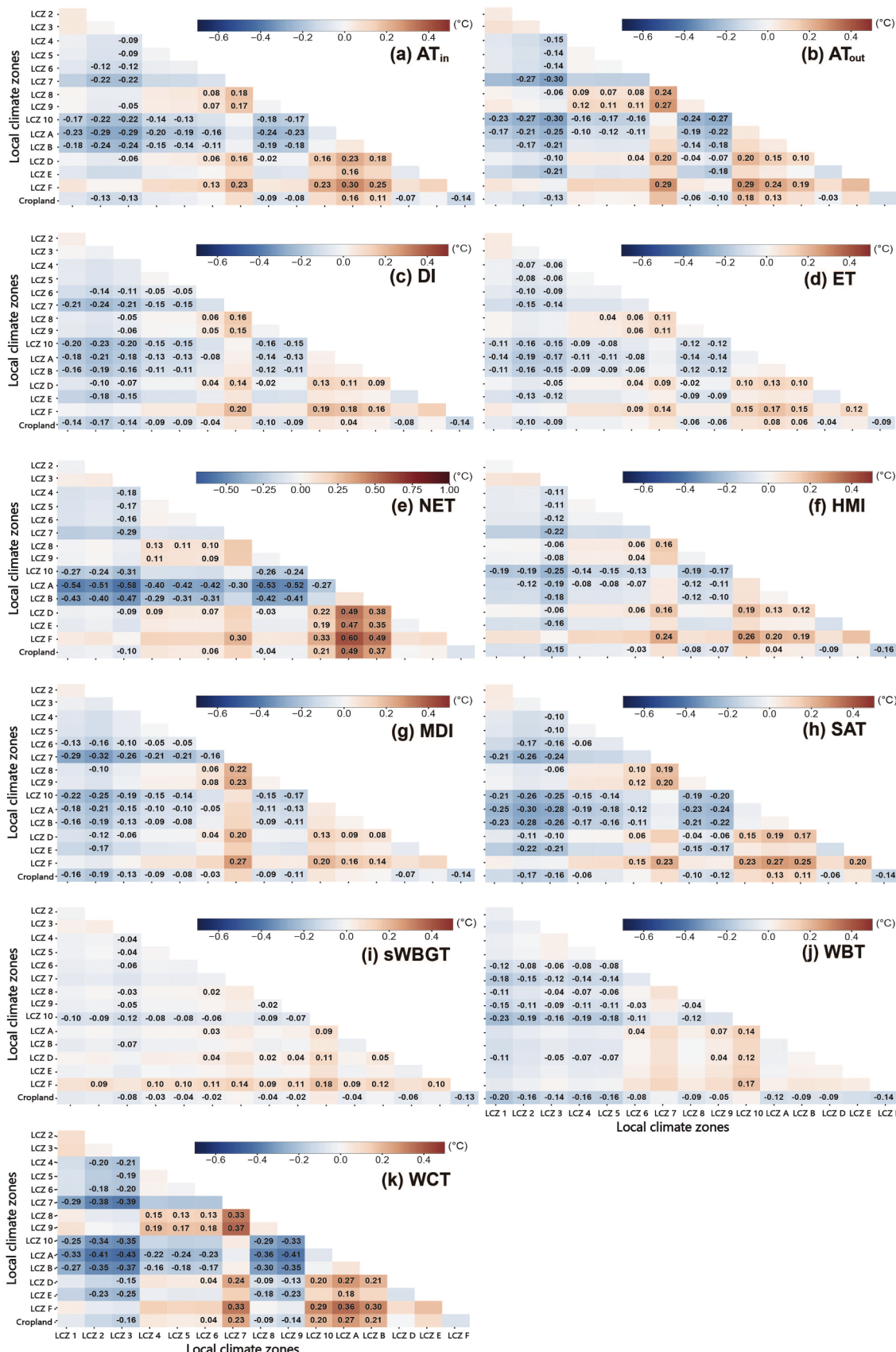


Fig. 10. Differences in the HPT changes under wintertime extreme cold weather across various LCZs in the urban areas of NCP from 2003 to 2020: (a) AT_{in} , (b) AT_{out} , (c) DI, (d) ET, (e) NET, (f) HMI, (g) MDI, (h) SAT, (i) sWGBT, (j) WBT, and (k) WCT. Black bolded values indicate a significant difference between the two types (i.e., the HPT change in one type in the row minus that in another one in the column) at the 0.05 level. For example, “-0.09” in (a) means that the AT_{in} drop during cold extremes in LCZ 4 is significantly stronger than that in LCZ 3 by 0.09°C .

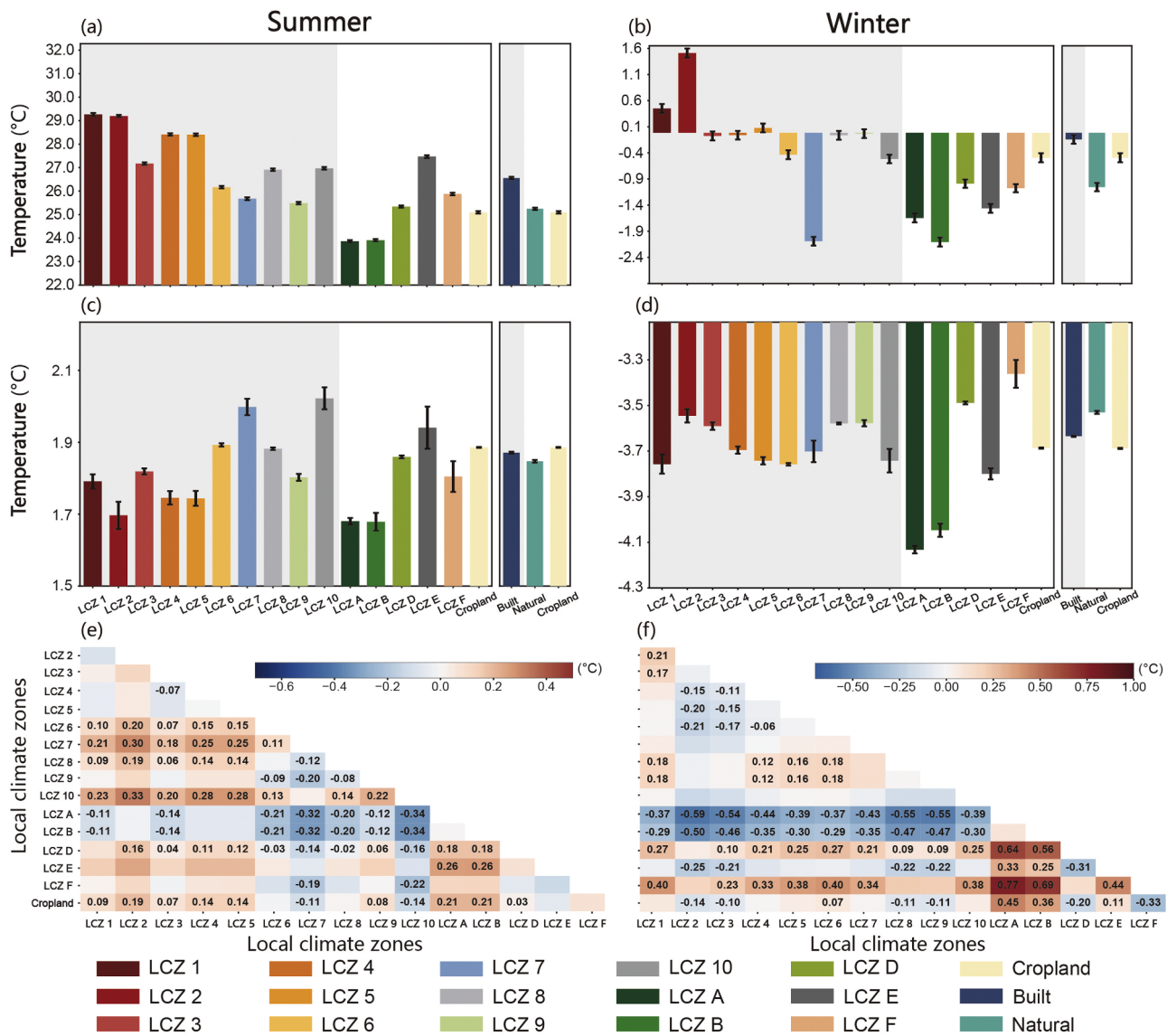


Fig. 11. Seasonal mean and changes of LST under extreme temperature events in various LCZs of NCP from 2003 to 2020. (a) and (b) represent the seasonal mean of summer LST and winter LST, respectively. The light gray background indicates HPT in built-up LCZs, and the white background indicates natural and cropland regions. HPT in different LCZs and cropland are shown in the bar plot on the left side. The LCZs are categorized into three main types (i.e., built area, natural land, and cropland), the HPT of which are shown on the right side. (c) and (d) denote the LST changes during summer extreme heat days and winter extreme cold days. (e) and (f) display the differences in the LST changes on summer extreme heat days and winter extreme cold days, respectively, among various LCZs. Black bolded values indicate the significant difference between two LCZ types (i.e., HPT change in one type in the row minus another type in the column) at the 0.05 level.

and bare rock areas (WCT of -3.71°C) have lower winter HPT.

Further investigations by comparing extreme and normal weather show that mid-rise building areas, with an HI change of 3.85°C , possibly due to their shading effects, experience smaller HPT increases than low-rise (4.10°C) and similar-height buildings in open-structure LCZs (4.04°C) when extreme hot weather comes. Urban trees can effectively mitigate summer heat environments in cities, but during extreme heat, densely planted tree areas may increase humidity via enhanced transpiration, thus potentially exacerbating humid heat threat to urban residents compared with sparsely planted trees (as measured by sWBGT and WBT). During wintertime extreme cold events, compact mid- to low-rise building areas have the smallest HPT decreases among all LCZs. Additionally, areas including LCZs 7 and 10, which have high thermal conductivity and albedo, exhibit low adaptability and high vulnerability to extreme temperatures, showing significant HPT variations under extreme weather conditions. These findings improve scientific understanding of local HPT changes in relation to LCZs and extreme weather,

assist in mitigating human thermal environments and urban planning, and enhance the resilience of densely populated and highly active urban areas to cope with extreme weather.

CRediT authorship contribution statement

Xiang Li: Writing – original draft, Visualization, Software, Methodology, Formal analysis, Data curation. **Ming Luo:** Writing – review & editing, Supervision, Project administration, Methodology, Investigation, Funding acquisition, Conceptualization. **Jianfeng Li:** Writing – review & editing, Investigation. **Sijia Wu:** Writing – review & editing, Visualization, Investigation. **Hui Zhang:** Writing – review & editing, Investigation. **Ziwei Huang:** Writing – review & editing. **Qiuting Wang:** Writing – review & editing. **Wenyue Cao:** Writing – review & editing. **Yu Tang:** Writing – review & editing. **Xiaoyu Wang:** Writing – review & editing.

Declaration of competing interest

The authors declare no conflicts of interest relevant to this study.

Acknowledgments

The authors are very grateful to all entities that provide data supporting to this work. This work is supported by the National Natural Science Foundation of China (no. 42371028) and the Guangzhou Science and Technology Program (no. 2024A04J6282).

Data availability

Data will be made available on request.

References

- Bechtel, B., & Daneke, C. (2012). Classification of local climate zones based on multiple earth observation data. *IEEE Journal of Selected Topics in Applied Earth Observations and Remote Sensing*, 5, 1191–1202. <https://doi.org/10.1109/JSTARS.2012.2189873>
- Bröde, P., Fiala, D., Blażejczyk, K., Holmér, I., Jendritzky, G., Kampmann, B., & Havenith, G. (2012). Deriving the operational procedure for the Universal Thermal Climate Index (UTCI). *International Journal of Biometeorology*, 56, 481–494. <https://doi.org/10.1007/s00484-011-0454-1>
- Chen, G., Chen, Y., He, H., Wang, J., Zhao, L., & Cai, Y. (2023). Assessing the synergies between heat waves and urban heat islands of different local climate zones in Guangzhou, China. *Building and Environment*, 240, Article 110434. <https://doi.org/10.1016/j.buildenv.2023.110434>
- Cheng, Q., Jin, H., & Ren, Y. (2023). Compound daytime and nighttime heatwaves for air and surface temperature based on relative and absolute threshold dynamic classified in Southwest China, 1980–2019. *Sustainable Cities and Society*, 91, Article 104433. <https://doi.org/10.1016/j.jscs.2023.104433>
- China Meteorological Administration. (2023). *Blue book on climate change in China (2023)*. Beijing: Science Press.
- Demuzere, M., Kittner, J., Martilli, A., Mills, G., Moede, C., Stewart, I. D., & Bechtel, B. (2022). A global map of local climate zones to support earth system modelling and urban-scale environmental science. *Earth System Science Data*, 14, 3835–3873. <https://doi.org/10.5194/essd-14-3835-2022>
- Dong, J., Hu, T., Liu, Y., & Peng, J. (2024). Urban-rural differences in the local human exposure to humid heatwaves in the Northern Hemisphere. *Sustainable Cities and Society*, 107, Article 105415. <https://doi.org/10.1016/j.jscs.2024.105415>
- Du, S., Kuang, X., Chen, J., Ye, Y., Li, P., & Shi, X. (2024). Development of an expanded local climate zone scheme to accommodate diversified urban morphological evolution: A case study of Shanghai, China. *Urban Climate*, 56, Article 102009. <https://doi.org/10.1016/j.uclim.2024.102009>
- Eptein, Y., & Moran, D. (2006). Thermal comfort and the heat stress indices. *Industrial Health*, 44, 388–398. <https://doi.org/10.2486/indhealth.44.388>
- Friedl, M., & Sulla-Menashe, D. (2022). MODIS/Terra+Aqua land cover type yearly L3 global 500m sin grid V061 [dataset]. N.E.P.D.A.A. Center. <https://doi.org/10.5067/MODIS/MCD12Q1.061>
- Gagge, A. P., Stolwijk, J., & Nishi, Y. (1971). An effective temperature scale based on a simple model of human physiological regulatory response. *ASHRAE Transactions*, 77, 247–262. <http://hdl.handle.net/2115/37901>
- Gaines, P. A., & Howell, J. F. (1976). Pairwise multiple comparison procedures with unequal N's and/or variances: A Monte Carlo study. *Journal of Educational Statistics*, 1, 113–125. <https://doi.org/10.3102/10769986001002113>
- Gao, H., Xia, X., Zhang, Z., Chen, J., & Liu, S. (2024). Temperature response of soil respiration decreases with latitude and elevation in abandoned croplands. *Agriculture, Ecosystems & Environment*, 363, Article 108862. <https://doi.org/10.1016/j.agee.2023.108862>
- García, D. H. (2022). Analysis of urban heat island and heat waves using Sentinel-3 Images: A study of andalusian cities in Spain. *Earth Systems and Environment*, 6, 199–219. <https://doi.org/10.1007/s41748-021-00268-9>
- Geletič, J., Lehnerth, M., Savić, S., & Milošević, D. (2018). Modelled spatiotemporal variability of outdoor thermal comfort in local climate zones of the city of Brno, Czech Republic. *Science of The Total Environment*, 624, 385–395. <https://doi.org/10.1016/j.scitotenv.2017.12.076>
- Geng, X., Zhang, D., Li, C., Yuan, Y., Yu, Z., & Wang, X. (2023). Impacts of climatic zones on urban heat island: Spatiotemporal variations, trends, and drivers in China from 2001 to 2020. *Sustainable Cities and Society*, 89. <https://doi.org/10.1016/j.jscs.2022.104303>
- Han, D., Wiesmeier, M., Conant, R. T., Kuhnel, A., Sun, Z., Kogel-Knabner, I., & Ouyang, Z. (2018). Large soil organic carbon increase due to improved agronomic management in the North China Plain from 1980s to 2010s. *Global Change Biology*, 24, 987–1000. <https://doi.org/10.1111/gcb.13898>
- He, B.-J., Ding, L., & Prasad, D. (2020). Relationships among local-scale urban morphology, urban ventilation, urban heat island and outdoor thermal comfort under sea breeze influence. *Sustainable Cities and Society*, 60, Article 102289. <https://doi.org/10.1016/j.jscs.2020.102289>
- Heidari, A., Davtalab, J., & Sargazi, M. A. (2024). Effect of awning on thermal comfort adjustment in open urban space using PET and UTCI indexes: A case study of Sistan region in Iran. *Sustainable Cities and Society*, 101, Article 105175. <https://doi.org/10.1016/j.jscs.2024.105175>
- Höppe, P. (1999). The physiological equivalent temperature - a universal index for the biometeorological assessment of the thermal environment. *International journal of biometeorology*, 43, 71–75. <https://doi.org/10.1007/s004840050118>
- Hou, H., Su, H., Yao, C., & Wang, Z.-H. (2023). Spatiotemporal patterns of the impact of surface roughness and morphology on urban heat island. *Sustainable Cities and Society*, 92. <https://doi.org/10.1016/j.jscs.2023.104513>
- Houghton, F. C., & Yaglou, C. P. (1923). Determining equal comfort lines. *J. Am. Soc. Heating and Ventilation in England*, 29, 165–176.
- IPCC. (2023). Climate change 2023: Synthesis report. A report of the Intergovernmental panel on climate change. In *contribution of working groups I, II and III to contribution to the sixth assessment report of the intergovernmental panel on climate change*. Cambridge University Press.
- Jendritzky, G., de Dear, R., & Havenith, G. (2012). UTCI—Why another thermal index? *International Journal of Biometeorology*, 56, 421–428. <https://doi.org/10.1007/s00484-011-0513-7>
- Jiang, H., Sun, Z., Guo, H., Xing, Q., Du, W., & Cai, G. (2022a). A standardized dataset of built-up areas of China's cities with populations over 300,000 for the period 1990–2015. *Big Earth Data*, 6, 103–126. <https://doi.org/10.1080/20964471.2021.1950351>
- Jiang, S., Zhan, W., Dong, P., Wang, C., Li, J., Miao, S., & Wang, C. (2022b). Surface air temperature differences of intra- and inter-local climate zones across diverse timescales and climates. *Building and Environment*, 222, Article 109396. <https://doi.org/10.1016/j.buildenv.2022.109396>
- Jiang, S., Zhan, W., Li, L., Wang, C., Dong, P., Wang, S., & Gao, Y. (2024). Contrasting moist heat across local climate zones in heat and non-heat waves: Insights from 29 Chinese metropolises. *Building and Environment*, 253, Article 111328. <https://doi.org/10.1016/j.buildenv.2024.111328>
- Jiang, S., Zhan, W., Yang, J., Liu, Z., Huang, F., Lai, J., & Lee, X. (2020). Urban heat island studies based on local climate zones: A systematic overview. *Acta Geographica Sinica*, 75, 1860–1878. <https://doi.org/10.11821/dlx202009004>
- Kang, S., & Eltahir, E. A. B. (2018). North China Plain threatened by deadly heatwaves due to climate change and irrigation. *Nature Communications*, 9, 2894. <https://doi.org/10.1038/s41467-018-05252-y>
- Karim, S., Iqbal, M. S., Ahmad, N., Ansari, M. S., Mirza, Z., Merdad, A., & Kumar, S. (2023). Gene expression study of breast cancer using Welch Satterthwaite *t*-test, Kaplan-Meier estimator plot and Huber loss robust regression model. *Journal of King Saud University - Science*, 35, Article 102447. <https://doi.org/10.1016/j.jksus.2022.102447>
- Karimimoshaver, M., & Shahrok, M. S. (2022). The effect of height and orientation of buildings on thermal comfort. *Sustainable Cities and Society*, 79, Article 103720. <https://doi.org/10.1016/j.jscs.2022.103720>
- Kendy, E., Molden, D. J., Steenhuis, T. S., Liu, C., & Wang, J. (2003). *Policies drain the north china plain: Agricultural policy and groundwater depletion in luancheng county, 1949–2000. I.R. reports*. International Water Management Institute.
- Kotharkar, R., & Dongarsane, P. (2024). Investigating outdoor thermal comfort variations across local climate zones in Nagpur, India, using ENVI-met. *Building and Environment*, 249, Article 111122. <https://doi.org/10.1016/j.buildenv.2023.111122>
- Kotharkar, R., Dongarsane, P., Ghosh, A., & Kotharkar, V. (2024). Numerical analysis of extreme heat in Nagpur city using heat stress indices, all-cause mortality and local climate zone classification. *Sustainable Cities and Society*, 101, Article 105099. <https://doi.org/10.1016/j.jscs.2023.105099>
- Lambin, E. F., Geist, H. J., & Lepers, E. (2003). Dynamics of land-use and land-cover change in tropical regions. *Annual Review of Environment and Resources*, 28, 205–241. <https://doi.org/10.1146/annurev.energy.28.050302.105459>
- Lau, K. K.-L., Chung, S. C., & Ren, C. (2019). Outdoor thermal comfort in different urban settings of sub-tropical high-density cities: An approach of adopting local climate zone (LCZ) classification. *Building and Environment*, 154, 227–238. <https://doi.org/10.1016/j.buildenv.2019.03.005>
- Li, J., Chen, Y. D., Gan, T. Y., & Lau, N.-C. (2018). Elevated increases in human-perceived temperature under climate warming. *Nature Climate Change*, 8, 43–47. <https://doi.org/10.1038/s41558-017-0036-2>
- Li, J., Niu, J., Mak, C. M., Huang, T., & Xie, Y. (2020). Exploration of applicability of UTCI and thermally comfortable sun and wind conditions outdoors in a subtropical city of Hong Kong. *Sustainable Cities and Society*, 52, Article 101793. <https://doi.org/10.1016/j.jscs.2019.101793>
- Li, L., Yao, N., Li, Y., Liu, D. L., Wang, B., & Ayantobo, O. O. (2019). Future projections of extreme temperature events in different sub-regions of China. *Atmospheric Research*, 217, 150–164. <https://doi.org/10.1016/j.atmosres.2018.10.019>
- Li, X., Luo, M., Zhao, Y., Zhang, H., Ge, E., Huang, Z., & Tang, Y. (2023). A daily high-resolution (1 km) human thermal index collection over the North China Plain from 2003 to 2020. *Scientific Data*, 10, 634. <https://doi.org/10.1038/s41597-023-02535-y>
- Lin, L., Ge, E., Liu, X., Liao, W., & Luo, M. (2018). Urbanization effects on heat waves in Fujian Province, Southeast China. *Atmospheric Research*, 210, 123–132. <https://doi.org/10.1016/j.atmosres.2018.04.011>
- Lin, L., Luo, M., Chan, T. O., Ge, E., Liu, X., Zhao, Y., & Liao, W. (2019). Effects of urbanization on winter wind chill conditions over China. *Science of The Total Environment*, 688, 389–397. <https://doi.org/10.1016/j.scitotenv.2019.06.145>
- Lin, P., Gou, Z., Lau, S. S.-Y., & Qin, H. (2017). The impact of urban design descriptors on outdoor thermal environment: A literature review. *Energies*, 10, 2151. <https://doi.org/10.3390/en1022151>
- Luo, M., & Lau, N.-C. (2019). Characteristics of summer heat stress in China during 1979–2014: Climatology and long-term trends. *Climate Dynamics*, 53, 5375–5388. <https://doi.org/10.1007/s00382-019-04871-5>

- Luo, M., & Lau, N.-C. (2021a). Increasing human-perceived heat stress risks exacerbated by urbanization in China: A comparative study based on multiple metrics. *Earth's Future*, 9, Article e2020EF001848. <https://doi.org/10.1029/2020EF001848>
- Luo, M., & Lau, N. C. (2021b). Increasing human-perceived heat stress risks exacerbated by urbanization in China: A comparative study based on multiple metrics. *Earth's Future*, 9, Article e2020EF001848. <https://doi.org/10.1029/2020ef001848>
- Luo, M., Lau, N.-C., & Liu, Z. (2022). Different mechanisms for daytime, nighttime, and compound heatwaves in southern China. *Weather and Climate Extremes*, 36, Article 100449. <https://doi.org/10.1016/j.wace.2022.100449>
- Luo, M., Wu, S., Lau, G. N.-C., Pei, T., Liu, Z., Wang, X., & Zhang, W. (2024). Anthropogenic forcing has increased the risk of longer-traveling and slower-moving large contiguous heatwaves. *Science Advances*, 10, eadl1598. <https://doi.org/10.1126/sciadv.adl1598>
- Ma, L., Huang, G., Johnson, B. A., Chen, Z., Li, M., Yan, Z., & Lian, D. (2023). Investigating urban heat-related health risks based on local climate zones: A case study of Changzhou in China. *Sustainable Cities and Society*, 91, Article 104402. <https://doi.org/10.1016/j.scs.2023.104402>
- Manob, D., & Arijit, D. (2020). Exploring the pattern of outdoor thermal comfort (OTC) in a tropical planning region of eastern India during summer. *Urban Climate*, 34, Article 100708. <https://doi.org/10.1016/j.ulclim.2020.100708>
- Masterton, J. M., & Richardson, F. A. (1979). *Humidex: A method of quantifying human discomfort due to excessive heat and humidity*. Downsview, Ont.: Environment Canada, Atmospheric Environment.
- Meehl, G. A., & Tebaldi, C. (2004). More intense, more frequent, and longer lasting heat waves in the 21st century. *Science (New York, N.Y.)*, 305, 994–997. <https://doi.org/10.1126/science.1098704>
- Mishra, V., Ambika, A. K., Asoka, A., Aadhar, S., Buzan, J., Kumar, R., & Huber, M. (2020). Moist heat stress extremes in India enhanced by irrigation. *Nature Geoscience*, 13, 722–728. <https://doi.org/10.1038/s41561-020-00650-8>
- Mora, C., Dousset, B., Caldwell, I. R., Powell, F. E., Geronimo, R. C., Bielecki, Coral R., & Trautenberg, C. (2017). Global risk of deadly heat. *Nature Climate Change*, 7, 501–506. <https://doi.org/10.1038/nclimate3322>
- Moran, D., Shapiro, Y., Epstein, Y., Matthew, W., & Pandolfi, K. (1998). A modified discomfort index (MDI) as an alternative to the wet bulb globe temperature (WBGT). In *Environmental Ergonomics VIII*.
- Murali, G., Iwamura, T., Meiri, S., & Roll, U. (2023). Future temperature extremes threaten land vertebrates. *Nature*, 615, 461–467. <https://doi.org/10.1038/s41586-022-05606-z>
- National Bureau of Statistics of China. (2022). *International statistical yearbook*. Beijing, China: China statistics press.
- Osczevski, R., & Bluestein, M. (2005). The new wind chill equivalent temperature chart. *Bulletin of the American Meteorological Society*, 86, 1453–1458. <https://doi.org/10.1175/bams-86-10-1453>
- Overland, J. E. (2021). Causes of the record-breaking pacific northwest heatwave, late June 2021. *Atmosphere*, 12, 1434. <https://doi.org/10.3390/atmos12111434>
- Palanisamy, P. A., Zawadzka, J., Jain, K., Bonafoni, S., & Tiwari, A. (2024). Assessing diurnal land surface temperature variations across landcover and local climate zones: Implications for urban planning and mitigation strategies on socio-economic factors. *Sustainable Cities and Society*, 116, Article 105880. <https://doi.org/10.1016/j.scs.2024.105880>
- Rahman, M. A., Dervishi, V., Moser-Reischl, A., Ludwig, F., Pretzsch, H., Rötzer, T., & Pauleit, S. (2021). Comparative analysis of shade and underlying surfaces on cooling effect. *Urban Forestry & Urban Greening*, 63, Article 127223. <https://doi.org/10.1016/j.ufug.2021.127223>
- Rahman, M. A., Franceschi, E., Pattnaik, N., Moser-Reischl, A., Hartmann, C., Paeth, H., & Pauleit, S. (2022). Spatial and temporal changes of outdoor thermal stress: Influence of urban land cover types. *Scientific Reports*, 12, 671. <https://doi.org/10.1038/s41982-021-04669-8>
- Rahmani, N., & Sharifi, A. (2025). Urban heat dynamics in Local Climate Zones (LCZs): A systematic review. *Building and Environment*, 267, Article 112225. <https://doi.org/10.1016/j.buildenv.2024.112225>
- Roshan, G., Arekhi, S., Bayganchi, Z., & Attia, S. (2024). Evaluation of the intensity of urban heat islands during heat waves using local climate zones in the semi-arid, continental climate of Tehran. *Urban Climate*, 56, Article 102079. <https://doi.org/10.1016/j.ulclim.2024.102079>
- Rothfusz, L. P., & Headquarters, N. S. R. (1990). *The heat index equation (or, more than you ever wanted to know about heat index)* (p. 9023). Fort Worth, Texas: National Oceanic and Atmospheric Administration, National Weather Service, Office of Meteorology. http://www.srh.noaa.gov/images/ffc/pdf/ta_htindx.PDF
- Samset, B. H., Zhou, C., Fuglestvedt, J. S., Lund, M. T., Marotzke, J., & Zelinka, M. D. (2023). Steady global surface warming from 1973 to 2022 but increased warming rate after 1990. *Communications Earth & Environment*, 4, 400. <https://doi.org/10.1038/s43247-023-01061-4>
- Shen, Y., Kong, W., Fei, F., Chen, X., Xu, Y., Huang, C., & Yao, J. (2024). Stereoscopic urban morphology metrics enhance the nonlinear scale heterogeneity modeling of UHI with explainable AI. *Urban Climate*, 56, Article 102006. <https://doi.org/10.1016/j.ulclim.2024.102006>
- Steadman, R. G. (1979). The assessment of sultriness. Part I: A temperature-humidity index based on human physiology and clothing science. *Journal of Applied Meteorology and Climatology*, 18, 861–873. [https://doi.org/10.1175/1520-0450\(1979\)018<0861:TAOSPI>2.0.CO;2](https://doi.org/10.1175/1520-0450(1979)018<0861:TAOSPI>2.0.CO;2)
- Steadman, R. G. (1984). A universal scale of apparent temperature. *Journal of Applied Meteorology and Climatology*, 23, 1674–1687. [https://doi.org/10.1175/1520-0450\(1984\)023<1674:AUSOAT>2.0.CO;2](https://doi.org/10.1175/1520-0450(1984)023<1674:AUSOAT>2.0.CO;2)
- Stewart, I. D., & Oke, T. R. (2012). Local climate zones for urban temperature studies. *Bulletin of the American Meteorological Society*, 93, 1879–1900. <https://doi.org/10.1175/bams-D-11-00019.1>
- Stone, B., Jr., Mallen, E., Rajput, M., Gronlund, C. J., Broadbent, A. M., Krayenhoff, E. S., & Georgescu, M. (2021). Compound climate and infrastructure events: How electrical grid failure alters heat wave risk. *Environmental Science & Technology*, 55, 6957–6964. <https://doi.org/10.1021/acs.est.1c0024>
- Stull, R. (2011). Wet-bulb temperature from relative humidity and air temperature. *Journal of Applied Meteorology and Climatology*, 50, 2267–2269. <https://doi.org/10.1175/jamc-D-11-0143.1>
- Thapa, S., Rijal, H. B., & Zaki, S. A. (2024). District-wise evaluation of meteorological factors and outdoor thermal comfort in India using UTCI – Insight into future climatic scenario. *Sustainable Cities and Society*, 116, Article 105840. <https://doi.org/10.1016/j.scs.2024.105840>
- Thorsson, S., Lindberg, F., Eliasson, I., & Holmer, B. (2007). Different methods for estimating the mean radiant temperature in an outdoor urban setting. *International Journal of Climatology*, 27, 1983–1993. <https://doi.org/10.1002/joc.1537>
- Tian, Y., Zhou, W., Qian, Y., Zheng, Z., & Yan, J. (2019). The effect of urban 2D and 3D morphology on air temperature in residential neighborhoods. *Landscape Ecology*, 34, 1161–1178. <https://doi.org/10.1007/s10980-019-00834-7>
- Top, S., Milošević, D., Caluwaerts, S., Hamdi, R., & Savić, S. (2020). Intra-urban differences of outdoor thermal comfort in Ghent on seasonal level and during record-breaking 2019 heat wave. *Building and Environment*, 185, Article 107103. <https://doi.org/10.1016/j.buildenv.2020.107103>
- Turner, V. K., Middel, A., & Vanos, J. K. (2023). Shade is an essential solution for hotter cities. *Nature*, 619, 694–697. <https://doi.org/10.1038/d41586-023-02311-3>
- Vargas Zeppetello, L. R., Raftery, A. E., & Battisti, D. S. (2022). Probabilistic projections of increased heat stress driven by climate change. *Communications Earth & Environment*, 3, 183. <https://doi.org/10.1038/s43247-022-00524-4>
- Verdonck, M. L., Coillie, F. V., Wulf, R. D., Okujeni, A., Linden, S.v.d., Demuzere, M., & Hooyberghs, H. (2017). Thermal evaluation of the local climate zone scheme in Belgium. In *2017 Joint Urban Remote Sensing Event (JURSE)*.
- Wan, W., Liu, Z., Li, J., Xu, J., Wu, H., & Xu, Z. (2022). Spatiotemporal patterns of maize drought stress and their effects on biomass in the Northeast and North China Plain from 2000 to 2019. *Agricultural and Forest Meteorology*, 315, Article 108821. <https://doi.org/10.1016/j.agrformet.2022.108821>
- Wang, A., Tao, H., Wu, Q., Huang, J., Zhang, B., & Wang, Y. (2022). Increasing urban and rural population exposures to warm-season concurrent hot days and nights on the North China Plain. *International Journal of Climatology*, 42, 7938–7950. <https://doi.org/10.1002/joc.7685>
- Wang, B., & Yi, Y. K. (2021). Developing an adapted UTCI (Universal Thermal Climate Index) for the elderly population in China's severe cold climate region. *Sustainable Cities and Society*, 69, Article 102813. <https://doi.org/10.1016/j.scs.2021.102813>
- Wang, C., Wang, Z.-H., Wang, C., & Myint, S. W. (2019a). Environmental cooling provided by urban trees under extreme heat and cold waves in U.S. cities. *Remote Sensing of Environment*, 227, 28–43. <https://doi.org/10.1016/j.rse.2019.03.024>
- Wang, F., Gao, M., Liu, C., Zhao, R., & McElroy, M. B. (2024). Uniformly elevated future heat stress in China driven by spatially heterogeneous water vapor changes. *Nature Communications*, 15, 4522. <https://doi.org/10.1038/s41467-024-48895-w>
- Wang, J., Wang, E., Feng, L., Yin, H., & Yu, W. (2013). Phenological trends of winter wheat in response to varietal and temperature changes in the North China Plain. *Field Crops Research*, 144, 135–144. <https://doi.org/10.1016/j.fcr.2012.12.020>
- Wang, J., Zhou, W., Jiao, M., Zheng, Z., Ren, T., & Zhang, Q. (2020). Significant effects of ecological context on urban trees' cooling efficiency. *ISPRS Journal of Photogrammetry and Remote Sensing*, 159, 78–89. <https://doi.org/10.1016/j.isprsjprs.2019.11.001>
- Wang, P., Li, D., Liao, W., Rigden, A., & Wang, W. (2019b). Contrasting evaporative responses of ecosystems to heatwaves traced to the opposing roles of vapor pressure deficit and surface resistance. *Water Resources Research*, 55, 4550–4563. <https://doi.org/10.1029/2019WR024771>
- Wang, P., Luo, M., Liao, W., Xu, Y., Wu, S., Tong, X., & Han, Y. (2021). Urbanization contribution to human perceived temperature changes in major urban agglomerations of China. *Urban Climate*, 38, Article 100910. <https://doi.org/10.1016/j.ulclim.2021.100910>
- Wei, X., Ye, Y., Zhang, Q., Li, B., & Wei, Z. (2019). Reconstruction of cropland change in North China Plain Area over the past 300 years. *Global and Planetary Change*, 176, 60–70. <https://doi.org/10.1016/j.gloplacha.2019.01.010>
- Welch, B. (1951). On the comparison of several mean values: An alternative approach. *Biometrika*, 38, 330–336. <https://doi.org/10.1093/biomet/38.3-4.330>
- Willett, K. M., & Sherwood, S. (2012). Exceedance of heat index thresholds for 15 regions under a warming climate using the wet-bulb globe temperature. *International Journal of Climatology*, 32, 161–177. <https://doi.org/10.1002/joc.2257>
- World Health Organization. (2018). *Health, environment and climate change: Human health and biodiversity: Report by the director-general*. World Health Organization.
- Wu, D., Fang, S., Li, X., He, D., Zhu, Y., Yang, Z., & Wu, Y. (2019a). Spatial-temporal variation in irrigation water requirement for the winter wheat-summer maize rotation system since the 1980s on the North China Plain. *Agricultural Water Management*, 214, 78–86. <https://doi.org/10.1016/j.agwat.2019.01.004>
- Wu, S., Liu, L., Gao, J., & Wang, W. (2019b). Integrate risk from climate change in China under global warming of 1.5 and 2.0 °C. *Earth's Future*, 7, 1307–1322. <https://doi.org/10.1029/2019EF001194>
- Xie, J., Zhou, S., Chung, L. C. H., & Chan, T. O. (2024). Evaluating land-surface warming and cooling environments across urban-rural local climate zone gradients in subtropical megacities. *Building and Environment*, 251, Article 111232. <https://doi.org/10.1016/j.buildenv.2024.111232>

- Xu, H., Li, C., Hu, Y., Kong, R., Wang, Q., & Zhou, Y. (2024). Long-term temporal and spatial divergence patterns of urban heat risk in the Beijing–Tianjin–Hebei urban agglomeration. *Urban Climate*, 56, Article 102085. <https://doi.org/10.1016/j.ulclim.2024.102085>
- Yamazaki, D., Ikeshima, D., Tawatari, R., Yamaguchi, T., O'Loughlin, F., Neal, J. C., & Bates, P. D. (2017). A high-accuracy map of global terrain elevations. *Geophysical Research Letters*, 44, 5844–5853. <https://doi.org/10.1002/2017gl072874>
- Yang, Z., Peng, J., Liu, Y., Jiang, S., Cheng, X., Liu, X., & Yu, X. (2023). GloUTCI-M: A global monthly 1 km universal thermal climate index dataset from 2000 to 2022. *Earth System Science Data Discuss*, 2023, 1–25. <https://doi.org/10.5194/essd-2023-379>
- Yilmaz, M., Kara, Y., Çulpan, H. C., Can, G., & Toros, H. (2023). Detection and regional analysis of heatwave characteristics in Istanbul. *Sustainable Cities and Society*, 97, Article 104789. <https://doi.org/10.1016/j.scs.2023.104789>
- Yilmaz, S., Toy, S., Irmak, M. A., & Yilmaz, H. (2007). Determination of climatic differences in three different land uses in the city of Erzurum, Turkey. *Building and Environment*, 42, 1604–1612. <https://doi.org/10.1016/j.buildenv.2006.01.017>
- You, Q., Chen, D., Wu, F., Pepin, N., Cai, Z., Ahrens, B., & AghaKouchak, A. (2020). Elevation dependent warming over the Tibetan Plateau: Patterns, mechanisms and perspectives. *Earth-Science Reviews*, 210, Article 103349. <https://doi.org/10.1016/j.earscirev.2020.103349>
- You, Q., Jiang, Z., Yue, X., Guo, W., Liu, Y., Cao, J., & Zhai, P. (2022). Recent frontiers of climate changes in east Asia at global warming of 1.5 °C and 2 °C. *njp Climate and Atmospheric Science*, 5, 80. <https://doi.org/10.1038/s41612-022-00303-0>
- Zhang, H., Luo, M., Pei, T., Liu, X., Wang, L., Zhang, W., & Liao, W. (2023a). Unequal urban heat burdens impede climate justice and equity goals. *The Innovation*, 4, Article 100488. <https://doi.org/10.1016/j.xinn.2023.100488>
- Zhang, H., Luo, M., Zhao, Y., Lin, L., Ge, E., Yang, Y., & Wang, X. (2023b). HiTIC-Monthly: A monthly high spatial resolution (1 km) human thermal index collection over China during 2003–2020. *Earth System Science Data*, 15, 359–381. <https://doi.org/10.5194/essd-15-359-2023>
- Zhang, J., Liu, Z., & Chen, L. (2015). Reduced soil moisture contributes to more intense and more frequent heat waves in northern China. *Advances in Atmospheric Sciences*, 32, 1197–1207. <https://doi.org/10.1007/s00376-014-4175-3>
- Zhang, J., You, Q., Ren, G., & Ullah, S. (2023c). Substantial increase in human-perceived heatwaves in eastern China in a warmer future. *Atmospheric Research*, 283, Article 106554. <https://doi.org/10.1016/j.atmosres.2022.106554>
- Zhang, L., Yang, L., Zohner, C. M., Crowther, T. W., Li, M., Shen, F., & Zhou, C. (2022a). Direct and indirect impacts of urbanization on vegetation growth across the world's cities. *Science Advances*, 8, eab0095. <https://doi.org/10.1126/sciadv.ab0095>
- Zhang, T., Zhou, Y., Zhu, Z., Li, X., & Asrar, G. R. (2022b). A global seamless 1 km resolution daily land surface temperature dataset (2003–2020). *Earth System Science Data*, 14, 651–664. <https://doi.org/10.5194/essd-14-651-2022>
- Zhang, Y., Qi, Y., Shen, Y., Wang, H., & Pan, X. (2019). Mapping the agricultural land use of the North China Plain in 2002 and 2012. *Journal of Geographical Sciences*, 29, 909–921. <https://doi.org/10.1007/s11442-019-1636-8>
- Zhao, C., Jensen, J. L. R., Weng, Q., Currit, N., & Weaver, R. (2020). Use of local climate zones to investigate surface urban heat islands in Texas. *GIScience & Remote Sensing*, 57, 1083–1101. <https://doi.org/10.1080/15481603.2020.1843869>
- Zhao, G. N., Li, B. Z., Kong, P., Xia, L. J., & Zhan, M. J. (2019). Population exposure to large-scale heatwaves in China for 1961–2015. *IOP Conference Series: Earth and Environmental Science*, 344, Article 012073. <https://doi.org/10.1088/1755-1315/344/1/012073>
- Zhou, D., Zhao, S., Liu, S., Zhang, L., & Zhu, C. (2014). Surface urban heat island in China's 32 major cities: Spatial patterns and drivers. *Remote Sensing of Environment*, 152, 51–61. <https://doi.org/10.1016/j.rse.2014.05.017>
- Zhou, L., Yuan, B., Hu, F., Wei, C., Dang, X., & Sun, D. (2022). Understanding the effects of 2D/3D urban morphology on land surface temperature based on local climate zones. *Building and Environment*, 208, Article 108578. <https://doi.org/10.1016/j.buildenv.2021.108578>
- Zhou, S., Li, M., & Xie, J. (2024). Evaluating urban-rural gradients and urban forms in metropolitan areas: A local climate zone approach with future spatial simulation. *Sustainable Cities and Society*, , Article 105636. <https://doi.org/10.1016/j.scs.2024.105636>
- Zhou, W., Wang, J., & Cadenasso, M. L. (2017). Effects of the spatial configuration of trees on urban heat mitigation: A comparative study. *Remote Sensing of Environment*, 195, 1–12. <https://doi.org/10.1016/j.rse.2017.03.043>